

REGULARIZED ESTIMATION OF MONGE-KANTOROVICH QUANTILES FOR SPHERICAL DATA

BERNARD BERCU, JÉRÉMIE BIGOT AND GAUTHIER THURIN

Université de Bordeaux

Institut de Mathématiques de Bordeaux et CNRS (UMR 5251)

ABSTRACT. Tools from optimal transport (OT) theory have recently been used to define a notion of quantile function for directional data. In practice, regularization is mandatory for applications that require out-of-sample estimates. To this end, we introduce a regularized estimator built from entropic optimal transport, by extending the definition of the entropic map to the spherical setting. We propose a stochastic algorithm to directly solve a continuous OT problem between the uniform distribution and a target distribution, by expanding Kantorovich potentials in the basis of spherical harmonics. In addition, we define the directional Monge-Kantorovich depth, a companion concept for OT-based quantiles. We show that it benefits from desirable properties related to Liu-Zuo-Serfling axioms for the statistical analysis of directional data. Building on our regularized estimators, we illustrate the benefits of our methodology for data analysis.

Keywords: Directional statistics; Monge-Kantorovich quantiles; Entropic Optimal Transport; Spherical harmonics; Fast Fourier transform.

AMS classifications: 62H11, 62G30, 62L20.

1. INTRODUCTION

1.1. Quantiles for directional data using optimal transport. In various situations, data are naturally associated to directions that belong to the circle or the unit d -sphere \mathbb{S}^{d-1} for $d \geq 2$. Such observations, referred to as directional data, can be found in various applications including wildfires [2], gene expressions [22], or cosmology [56] to name but a few. Directional statistics [48, 49, 55, 68] is the field that brings together the corresponding models, methods and applications for statistical inference.

In this paper, we focus on the concept of quantiles for directional data. For real random variables, the notion of quantile is a well established statistical concept thanks to the canonical ordering of observations on the real line. Beyond the setting

The authors gratefully acknowledge financial support from the Agence Nationale de la Recherche (MaSDOL grant ANR-19-CE23-0017).

of distributions with rotational symmetry [47], the absence of a canonical ordering on \mathbb{S}^{d-1} makes the definition of quantiles for directional data more involved.

A recent line of research in nonparametric statistics [11, 34, 35, 37] deals with the use of the theory of optimal transport (OT) to define Monge-Kantorovich (MK) quantiles¹ for multivariate data. Desirable properties of MK quantiles include ancillarity, distribution-freeness of associated ranks, and consistence with the univariate setting [35], together with connections to the celebrated Tukey’s notion of statistical depth [11] and Mahalanobis distance [33]. The concept of MK quantiles has also proven to be fruitful in many applications, including statistical testing [30, 39, 63, 74, 75], regression [9, 18], risk measurement [4], and Lorenz maps [23, 38].

This approach has recently been applied in [37] to obtain a new notion of center-outward quantiles for directional data. Starting from independent and identically distributed (*i.i.d.*) directional data X_1, \dots, X_n sampled from a target measure ν , the main idea in [37] is to define an empirical quantile function \mathbf{Q}_n as an optimal matching. This is obtained by solving an OT problem between the empirical measure $\hat{\nu}_n = \frac{1}{n} \sum_{i=1}^n \delta_{X_i}$ and a uniform distribution $\mu_n = \frac{1}{n} \sum_{i=1}^n \delta_{U_i}$ based on a regular grid $\{U_1, \dots, U_n\}$ over the unit sphere \mathbb{S}^{d-1} . In this manner, if U is sampled from μ_n , the random vector $\mathbf{Q}_n(U)$ follows the empirical distribution of the observations, which is consistent with the standard univariate quantile function. On the other hand, the ranks of X_1, \dots, X_n follow the uniform distribution μ_n , independently from ν , which means that they are *distribution-free*. Building upon this property, [37] investigate rank-based statistical testing. However, the resulting matching between two discrete distributions does not provide out-of-sample estimates.

In contrast, this paper focuses on applications of MK quantiles where one is interested in observations X_{new} different from X_1, \dots, X_n . We give two examples that motivate our upcoming contributions. For depth-based classification, the depth (or outlyingness) of a testing point X_{new} must be computed after learning on training data X_1, \dots, X_n . For dispersion measurements, volumes of quantile regions \mathbb{C}_τ can be estimated by rejection sampling, repeatedly considering the event $\{X_{\text{new}} \in \mathbb{C}_\tau\}$.

1.2. Main contributions. To compute out-of-sample estimates, we pursue regularized estimation of directional MK quantiles. To do so, we rely on entropically regularized OT [15], that is well-known for its computational advantages. While the computational cost of solving a discrete OT problem is known to scale cubically in the number of observations [17], entropic regularization improves this to quadratic complexity.

A stochastic algorithm. We suggest to adapt the stochastic algorithm developed in [6] dealing with multivariate data in \mathbb{R}^d , that is not assumed to belong to the unit d -sphere. By expanding Kantorovich dual potentials in their series of Fourier coefficients, each iteration of the stochastic algorithm in [6] reduces to the use of the

¹These are also referred to as center-outward quantiles, [35].

Fast Fourier Transform (FFT). On the sphere \mathbb{S}^2 , dual potentials can be parameterized via spherical harmonics coefficients instead, that is the analog of the Fourier basis for square-integrable functions on \mathbb{S}^2 . In this manner, using a sequence of random variables X_1, \dots, X_n sampled from a target distribution ν supported on \mathbb{S}^2 , we construct a stochastic algorithm in the space of spherical harmonics coefficients. In practice, this algorithm depends on the choice of a grid of points in \mathbb{S}^2 of size $\mathcal{O}(p^2)$ to implement a FFT on \mathbb{S}^2 [84]. The computational cost at each iteration is thus of order $\mathcal{O}(p^2 \log^2(p))$ [46]. A key motivation for such stochastic algorithm is its ability to solve OT in an online fashion, where data arrives sequentially. Also, it overcomes the need to discretize the reference distribution, by learning directly the continuous OT problem.

A regularized quantile function. Furthermore, we also derive an estimator of the quantile function for spherical data that is smoother than \mathbf{Q}_n . This regularized quantile function is a directional counterpart of the *entropic map* [69], following classical results on entropic optimal transport in the euclidean space \mathbb{R}^d . Its main benefit, beyond computational complexity, is to allow for out-of-sample estimation.

Directional statistical depth. Finally, we introduce the new notion of MK directional statistical depth, in accordance with the euclidean MK depth [11]. We discuss its properties relative to traditional Liu-Zuo-Serfling axioms for the statistical analysis of directional data. Moreover, we study statistical applications built from it, and provide a comparison with other estimators, to better highlight the potential of entropic regularization for spherical quantiles estimation and out-of-sample estimation.

1.3. Organization of the paper. In Section 2, we discuss related works on alternative definitions and estimators of quantiles for directional data. The definitions of OT-based directional distribution and quantile functions on \mathbb{S}^2 are recalled in Section 3. Our approach to obtain regularized estimators of MK quantiles on \mathbb{S}^2 is detailed in Section 4. A study of the MK directional statistical depth, is proposed in Section 5 and illustrated with simulated data. Numerical experiments are reported in Section 6 to highlight the benefits of entropic regularization. Concluding remarks and discussions on this work are proposed in Section 7. Finally, mathematical details and proofs are deferred to technical appendices. Python codes for the experiments carried out in this paper are available at <https://github.com/gauthierthurin/SphericalQuantiles>.

2. RELATED WORKS

2.1. Directional quantiles and depth. Very much related to multivariate quantiles is the idea of statistical depth and the center-outward ordering of data, with a long history dating back to Tukey’s work [78]. The issue of *picturing data*, in Tukey’s terminology, has since gained very much attention, which prevents us from providing an exhaustive survey, and we rather refer to [3, 51, 60, 73]. The first notion of directional depth function was introduced in [76], followed by the work of [52] that developed

three different approaches. The properties of the latter have been studied and applied for inference in [1, 70]. The required computational effort led the authors of [47] to build the angular Mahalanobis depth, and, doing so, they provided the first concept of directional quantiles. Despite appealing properties, the obtained contours are constrained to be rotationally symmetric, motivating the elliptic counterpart from [41]. Still, the elliptic assumption is a strong one as discussed in [37]. Facing either this lack of adaptiveness or the computational burdens of previous references, distance-based depths were proposed in [66], even though not explicitly related to the notion of quantiles. These directional depth functions can be applied, for instance, in data analysis and inference [1, 45, 52, 76], classification [20, 21, 45, 52, 61, 66] or clustering [65]. Among recent years, two concepts of multivariate quantiles have emerged in \mathbb{R}^d , namely the spatial quantiles [10] and the center-outward ones [11], both gathering most of commonly sought-after properties. More importantly here, these promising ideas have successfully been extended to directional data [37, 45], improving on the lack of adaptiveness of Mahalanobis quantiles [47], with desirable asymptotic results inherited from the formalism of quantiles.

To put it in a nutshell, existing concepts of directional quantiles include Mahalanobis quantiles, Spatial quantiles and Monge-Kantorovich ones. On the one hand, a statistical depth associated to a notion of quantiles is amenable to benefit from the best of both worlds, that is adaptivity to the underlying geometry and consistency of empirical versions, as argued for instance in [45]. On another hand, in comparison with other directional quantiles, Monge-Kantorovich ones present an additional descriptive power inherited from the fact that $\mathbf{Q}(U) \sim \nu$. A direct consequence is that \mathbf{Q} must contain all the available information, which is appealing with the purpose of summing up unknown features of multivariate data. Lastly, we mention that the estimation of density level sets on \mathbb{S}^{d-1} , [71], is a related but different objective. Indeed, the density allows to capture local information such as multimodality (as with a histogram) while quantiles focus on a global centrality information (as with a boxplot).

2.2. Regularized OT maps on the sphere. In [37], the estimation of directional quantiles amounts to a discrete OT problem. However, such estimator is piecewise constant, restricted to take its values in the set of observations. There, regularization naturally enters the picture, as highlighted in \mathbb{R}^d in several works, either after the estimation of unregularized OT [4, 35], or with entropic optimal transport (EOT) [6, 9, 57]. Facing the same issue in the present directional context, the entropic map is extended here to the non-Euclidean setting, similarly to what is done in [16] for general costs in \mathbb{R}^d . To the best of our knowledge, this appears to be new, although it benefits from explicit formulation tractable in linear time, given the dual potentials solving EOT. This belongs to the line of work estimating OT maps on manifolds. A meaningful approach is to use deep-learning architectures [13]. In particular, [67] extends [37] to vector quantile regression on manifolds, with convincing numerical performance. Some works leverage mesh adaptation [83] or PDE [40].

The recent theoretical work [26] provides complete convergence result, building on an interesting idea of discrete OT maps through geometric medians, akin to the barycentric projection in \mathbb{R}^d . Following insights from previous works on Euclidean data [6, 9, 57], EOT in the quantiles' context is a complementary perspective that enforces smoothness, to fulfill our objective of depth-based data analysis.

3. DIRECTIONAL DISTRIBUTION AND QUANTILE FUNCTIONS ON THE 2-SPHERE BASED ON OPTIMAL TRANSPORT

In this section, we introduce the main definitions of OT-based distribution and quantile functions for spherical data, beginning with notation related to spherical harmonics and differentiation on \mathbb{S}^2 .

3.1. Context. The unit 2-sphere is defined by $\mathbb{S}^2 = \{x \in \mathbb{R}^3 : \|x\| = 1\}$. The points $x \in \mathbb{S}^2$ can be written in spherical coordinates, with longitude $\phi \in [-\pi, \pi]$ and colatitude $\theta \in [0, \pi]$, as

$$(3.1) \quad x = \Phi(\theta, \phi) := (\cos \phi \sin \theta, \sin \phi \sin \theta, \cos \theta).$$

On the 2-sphere, the geodesic distance is $d(x, y) = \arccos(\langle x, y \rangle)$, and the squared Riemannian distance is

$$(3.2) \quad c(x, y) = \frac{1}{2}d(x, y)^2.$$

Both d and c are continuous and bounded as $d(x, y) \in [0, \pi]$. Moreover, (\mathbb{S}^2, d) is a separable complete metric space, with Borel algebra \mathcal{B}^2 . The surface measure $\sigma_{\mathbb{S}^2}$ on \mathbb{S}^2 is given by

$$\int_{\mathbb{S}^2} f(x) d\sigma_{\mathbb{S}^2}(x) = \int_0^\pi \int_{-\pi}^\pi f(\Phi(\theta, \phi)) \sin \theta d\phi d\theta,$$

and the uniform measure on \mathbb{S}^2 writes $\mu_{\mathbb{S}^2} = \frac{1}{4\pi}\sigma_{\mathbb{S}^2}$. The space of all equivalence classes of square integrable functions on \mathbb{S}^2 is denoted by $L^2(\mathbb{S}^2)$. We define the *spherical harmonic* function of degree $l \in \mathbb{N}^*$ and order $m \in \{-l, \dots, l\}$ by

$$Y_l^m(x) = Y_l^m(\Phi(\theta, \phi)) = \sqrt{\frac{2l+1}{4\pi} \frac{(l-m)!}{(l+m)!}} P_l^m(\cos \theta) e^{im\phi},$$

where the associated Legendre functions $P_l^m : [-1, 1] \rightarrow \mathbb{R}$ verify, for $l \in \mathbb{N}^*$ and $m \geq 0$,

$$P_l^m(t) = \frac{(-1)^m}{2^l l!} (1-t^2)^{m/2} \frac{d^{l+m}(t^2-1)^l}{dt^{l+m}} \quad \text{and} \quad P_l^{-m}(t) = (-1)^m \frac{(l-m)!}{(l+m)!} P_l^m(t).$$

Importantly, the spherical harmonics form an orthonormal basis of $L^2(\mathbb{S}^2)$, so that every function $f \in L^2(\mathbb{S}^2)$ is uniquely decomposed, for $x \in \mathbb{S}^2$, as

$$(3.3) \quad f(x) = \sum_{l=0}^{\infty} \sum_{m=-l}^l \bar{f}_l^m Y_l^m(x),$$

where the sequence of spherical harmonic coefficients $\bar{f} = (\bar{f}_l^m)$ verifies

$$(3.4) \quad \bar{f}_l^m = \frac{1}{4\pi} \int_{\mathbb{S}^2} f(x) \overline{Y_l^m(x)} d\sigma_{\mathbb{S}^2}(x).$$

We refer to [12] for an introduction to Fourier analysis on the sphere. Below, we introduce a few notation from differential geometry that one can find for instance in [24]. At any point $x \in \mathbb{S}^2$, the tangent space is $\mathcal{T}_x\mathbb{S}^2 = \{y \in \mathbb{R}^3 : \langle x, y \rangle = 0\}$, and the associated orthogonal projection $\rho_x : \mathbb{R}^3 \rightarrow \mathcal{T}_x\mathbb{S}^2$ verifies

$$(3.5) \quad \rho_x \xi = (I - xx^T)\xi = \xi - \langle \xi, x \rangle x.$$

The exponential map at $x \in \mathbb{S}^2$, $\text{Exp}_x : \mathcal{T}_x\mathbb{S}^2 \rightarrow \mathbb{S}^2$, has the explicit form

$$\text{Exp}_x(v) = \cos(\|v\|)x + \sin(\|v\|) \frac{v}{\|v\|},$$

and its inverse Log_x writes

$$(3.6) \quad \text{Log}_x(z) = \frac{d(x, z)}{\sqrt{1 - \langle x, z \rangle^2}} \rho_x z = d(x, z) \frac{\rho_x(z - x)}{\|\rho_x(z - x)\|}.$$

The Riemannian gradient is given by orthogonally projecting Euclidean derivatives onto the tangent space. For a smooth function $f : \mathbb{S}^2 \rightarrow \mathbb{R}$, its Riemannian gradient $\nabla f(x)$ at x is thus defined by

$$(3.7) \quad \nabla f(x) = \rho_x Df(x), \quad \text{where} \quad Df(x) = \left(\frac{\partial f(x)}{\partial x_i} \right)_{i,j \in \{1,2,3\}}.$$

The Riemannian Hessian $\nabla^2 f(x) : \mathcal{T}_x\mathbb{S}^2 \rightarrow \mathcal{T}_x\mathbb{S}^2$ at x is defined by the same token,

$$(3.8) \quad \nabla^2 f(x) = \rho_x \left[D^2 f(x) - \langle Df(x), x \rangle I \right] \quad \text{with} \quad D^2 f(x) = \left(\frac{\partial^2 f(x)}{\partial x_i \partial x_j} \right)_{i,j \in \{1,2,3\}}.$$

3.2. Main definitions. Here, we fix the definitions introduced in [37]. Given μ and ν two probability measures supported on \mathbb{S}^2 , we say that T pushes forward μ to ν , denoted by $T_{\#}\mu = \nu$, if, for each measurable $B \in \mathcal{B}^2$, $\nu(B) = \mu(T^{-1}(B))$. Then, for the quadratic cost c defined in (3.2), Monge's formulation of the OT problem between μ and ν writes

$$(3.9) \quad \min_{T: T_{\#}\mu = \nu} \mathbb{E}_{X \sim \mu} [c(X, T(X))].$$

The solution of (3.9) is referred to as a *Monge map*, while μ and ν are called the *reference* and *target* measures, respectively. Before considering the existence of Monge maps, we recall the key definition of c -transforms as stated in [58], that is equivalent to the formulation of [37][Definition 2].

Definition 3.1. *Given a function $\psi : \mathbb{S}^2 \rightarrow \mathbb{R}$, its c -transform is defined by $\psi^c(y) = \inf_{x \in \mathbb{S}^2} \{c(x, y) - \psi(x)\}$. Then, ψ is said to be c -concave when $\psi^{cc} := (\psi^c)^c = \psi$.*

The proper summary of [37][Proposition 1] highlights that c -concavity is related to optimality in Monge's OT problem (3.9). For our continuous and bounded cost c , a sufficient assumption is that the reference measure belongs to \mathbf{B}_2 , the family of $\sigma_{\mathbb{S}^2}$ -absolutely continuous distributions with densities bounded away from 0 and ∞ , see [58][Theorem 9], which is the case for the uniform $\mu_{\mathbb{S}^2}$. This enables the definition of distribution and quantile functions in [37].

Definition 3.2. *The directional MK quantile function of the arbitrary probability measure ν is the $\mu_{\mathbb{S}^2}$ -a.s. unique map $\mathbf{Q} : \mathbb{S}^2 \rightarrow \mathbb{S}^2$ such that $\mathbf{Q}_{\#}\mu_{\mathbb{S}^2} = \nu$ and there exists a c -concave differentiable mapping $\psi : \mathbb{S}^2 \rightarrow \mathbb{R}$ such that, $\sigma_{\mathbb{S}^2}$ -a.e.,*

$$\mathbf{Q}(x) = \text{Exp}_x(-\nabla\psi(x)).$$

In addition, the directional MK distribution function of ν is given by

$$\mathbf{F}(x) = \text{Exp}_x(-\nabla\psi^c(x)).$$

As soon as ν belongs to \mathbf{B}_2 , [58][Corollary 10] ensures that $\mathbf{F} = \mathbf{Q}^{-1}$ almost everywhere, whereas \mathbf{Q}^{-1} might not exist if ν is not absolutely continuous.

Remark 3.1 (Regularity). *The regularity of OT maps on the sphere is a delicate subject that has inspired a number of works, [19, 53, 54, 82]. Any c -concave potential ψ is twice differentiable almost everywhere [14][Proposition 3.14]. For further regularity, an appropriate requirement is that the underlying measures are smooth and belong to \mathbf{B}_2 . In particular, if, a minima, ν has density $f \in C^{1,1}(\mathbb{S}^2)$ with respect to $\sigma_{\mathbb{S}^2}$, then the MK quantile function \mathbf{Q} belongs to $C^{2,\beta}(\mathbb{S}^2)$ for all $\beta \in]0, 1[$, [54].*

In view of the proof of [58][Theorem 9], ψ and its c -transform ψ^c in Definition 3.2 maximize the dual version of Kantorovich's problem, in the sense that

$$(3.10) \quad (\psi, \psi^c) \in \arg \max_{(u,v) \in \text{Lip}_c} \int_{\mathbb{S}^2} u(x) d\mu_{\mathbb{S}^2}(x) + \int_{\mathbb{S}^2} v(y) d\nu(y),$$

with $\text{Lip}_c = \{u, v : \mathbb{S}^2 \rightarrow \mathbb{R} \text{ continuous} ; u(x) + v(y) \leq c(x, y)\}$. The semi-dual version of (3.10) refers to the optimisation over a single dual variable u , the other being taken as u^c .

A central point in \mathbb{S}^2 must be chosen for the reference $\mu_{\mathbb{S}^2}$, to define nested regions with $\mu_{\mathbb{S}^2}$ -probability $\tau \in [0, 1]$. A well-suited notion of central point is the Fréchet median²

$$(3.11) \quad \theta_M = \arg \min_{z \in \mathbb{S}^2} \mathbb{E}_{Z \sim \nu} [d(Z, z)],$$

that can be computed with the package *geomstats* [59]. Then, the spherical cap with $\mu_{\mathbb{S}^2}$ -probability $\tau \in [0, 1]$ centered at $\mathbf{F}(\theta_M)$ is

$$\mathbb{C}_\tau^U = \{x \in \mathbb{S}^2 : \langle x, \mathbf{F}(\theta_M) \rangle \geq 1 - 2\tau\},$$

²This choice is motivated by its simplicity, and it implicitly assumes that the Fréchet median is unique. However, this may not be the case, even at the population level. For instance, this happens if ν charges antipodal regions equally.

with boundary $\mathcal{C}_\tau^U = \{x \in \mathbb{S}^2 : \langle x, \mathbf{F}(\theta_M) \rangle = 1 - 2\tau\}$ a *parallel* of order τ . This defines a rotated version of the usual latitude-longitude coordinate system (A.2), with respect to the pole $\mathbf{F}(\theta_M)$, as follows. Any $x \in \mathbb{S}^2$ decomposes into

$$(3.12) \quad x = \langle x, \mathbf{F}(\theta_M) \rangle \mathbf{F}(\theta_M) + \sqrt{1 - \langle x, \mathbf{F}(\theta_M) \rangle^2} \mathbf{S}_{\mathbf{F}(\theta_M)}(x),$$

where $\langle x, \mathbf{F}(\theta_M) \rangle$ is a latitude³ on the parallel \mathcal{C}_τ^U , while the *directional sign*

$$(3.13) \quad \mathbf{S}_{\mathbf{F}(\theta_M)}(x) = \frac{x - \langle x, \mathbf{F}(\theta_M) \rangle \mathbf{F}(\theta_M)}{\|x - \langle x, \mathbf{F}(\theta_M) \rangle \mathbf{F}(\theta_M)\|}$$

is a longitude, with convention $\mathbf{0}/0 = \mathbf{0}$ for $x = \pm \mathbf{F}(\theta_M)$. $\mathbf{S}_{\mathbf{F}(\theta_M)}(x)$ takes values on the rotated equator $\mathcal{C}_{1/2}^U$, and thus characterizes meridians crossing $s \in \mathcal{C}_{1/2}^U$ through $\mathcal{M}_s^U = \{x \in \mathbb{S}^2 : \mathbf{S}_{\mathbf{F}(\theta_M)}(x) = s\}$. The image by \mathbf{Q} of the parallel / meridian system (3.12) provides curvilinear parallels $\mathbf{Q}(\mathcal{C}_\tau^U)$ and curvilinear meridians $\mathbf{Q}(\mathcal{M}_s^U)$ adapted to the geometry of the support of ν , giving rise to suitable directional concepts of quantile contours and signs [37]. Intuitively, a change in coordinates in a data-adaptive fashion must retain all the available information, in a simpler form amenable to be summed up.

Definition 3.3 (Quantile contours, regions and signs). *Let $\nu \in \mathbf{B}_2$, with directional quantile function \mathbf{Q} . Then,*

- *the quantile contour of order $\tau \in [0, 1]$ is $\mathcal{C}_\tau = \mathbf{Q}(\mathcal{C}_\tau^U)$,*
- *the quantile region of order $\tau \in [0, 1]$ is $\mathbb{C}_\tau = \mathbf{Q}(\mathbb{C}_\tau^U)$,*
- *the sign curve associated with $s \in \mathcal{C}_{1/2}^U$ is $\mathbf{Q}(\mathcal{M}_s^U)$.*

Since \mathbf{Q} is a push-forward mapping, $\mathbf{Q}_\# \mu_{\mathbb{S}^2} = \nu$, the ν -probability content of \mathbb{C}_τ is τ . Moreover, the quantile contours of $\nu \in \mathbf{B}_2$ are continuous and the quantile regions are closed, connected and nested, as stated in [37].

4. REGULARIZED ESTIMATION

4.1. Entropic OT on the 2-sphere. We now introduce an algorithm based on the spherical Fourier transform to solve the regularized Kantorovich problem on the 2-sphere. In the Euclidean case, Kantorovich's problem is known to be easier to solve than Monge's problem [17]. Even more so, adding an entropic regularization term to (3.10) has been a cornerstone for the development of OT-based methods in statistics, [15]. For online learning, [29] proposed stochastic algorithms by rewriting the dual objective function, with convergence guarantees [5]. For arbitrary measures, (not only discrete ones), the dual variables cannot be viewed as finite-dimensional vectors anymore. Therefore, one requires the use of nonparametric families of dual functions. For Euclidean data in \mathbb{R}^d , one can use reproducing kernel Hilbert spaces [29], deep neural networks [72] or Fourier series [6]. For directional data in \mathbb{S}^{d-1} , we leverage spherical harmonics. The resulting algorithm directly targets the continuous OT

³The example $\mathbf{F}(\theta_M) = (0, 0, 1)^T$ eases the understanding: $x \in \mathcal{C}_\tau^U$ implies $\langle x, \mathbf{F}(\theta_M) \rangle = x_3 = 1 - 2\tau$ and the latitude is fixed.

problem between the continuous reference measure and the underlying ν in an online fashion, instead of the (semi) discrete OT problem towards the empirical measure $\hat{\nu}_n$. Also, the Network simplex and Sinkhorn algorithm require the storage of the cost matrix, of size n^2 for two samples of sizes n , whereas stochastic algorithms are designed to avoid it.

For spherical quantiles, one must solve an OT problem where the reference measure is $\mu_{\mathbb{S}^2}$, the uniform probability measure on the sphere. The semi-dual version of EOT between $\mu_{\mathbb{S}^2}$ and ν from [28][Proposition 12], for $\varepsilon > 0$ a regularization parameter, writes

$$(4.1) \quad \max_{u \in L^\infty(\mathbb{S}^2)} \int_{\mathbb{S}^2} u(x) d\mu_{\mathbb{S}^2}(x) + \int_{\mathbb{S}^2} u^{c,\varepsilon}(y) d\nu(y),$$

with $u^{c,\varepsilon}$ the *smooth conjugate* of u defined by

$$(4.2) \quad u^{c,\varepsilon}(y) = -\varepsilon \log \left(\int_{\mathbb{S}^2} \exp \left(\frac{u(x) - c(x,y)}{\varepsilon} \right) d\mu_{\mathbb{S}^2}(x) \right).$$

The smooth conjugate is the entropic counterpart of Definition 3.1. For bounded costs, the problem (4.1) admits a solution in L^∞ , unique up to additive constants, [28][Theorem 7]. To leverage unicity, we impose that $\int_{\mathbb{S}^2} u(x) d\mu_{\mathbb{S}^2}(x) = 0$, so that the optimisation problem (4.1) becomes

$$\max_{u \in L^\infty(\mathbb{S}^2)} \int_{\mathbb{S}^2} u^{c,\varepsilon}(y) d\nu(y).$$

It is well-known, [29, 64], that \mathbf{u}_ε is solution of (4.1) if and only if

$$(4.3) \quad \mathbf{u}_\varepsilon = ((\mathbf{u}_\varepsilon)^{c,\varepsilon})^{c,\varepsilon}.$$

Rewriting the problem. A Lipschitz continuous function on \mathbb{S}^2 equals its spherical Fourier series (3.3) pointwise [81][Theorem 5.26]. One can find in [58][Lemma 2] that the true unregularized potentials are Lipschitz, because \mathbb{S}^2 has a finite diameter $|\mathbb{S}^2| = \pi$. The same holds in the regularized case $\varepsilon > 0$, from the optimality condition (4.3), see Proposition 12 from [25][Appendix B] or [64][Lemma 3.1]. Consequently, we suggest to parameterize the dual variable in (4.1) by its spherical harmonic coefficients. For a given $\varepsilon > 0$, we consider the optimal sequence of coefficients $\bar{\mathbf{u}}_\varepsilon$ defined as the solution of the following *stochastic convex minimisation* problem

$$(4.4) \quad \bar{\mathbf{u}}_\varepsilon = \arg \min_{\bar{\mathbf{u}} \in \ell_1} H_\varepsilon(\bar{\mathbf{u}}) \quad \text{with} \quad H_\varepsilon(\bar{\mathbf{u}}) = \mathbb{E} [h_\varepsilon(\bar{\mathbf{u}}, X)]$$

where X is a random vector with distribution ν , $\bar{\mathbf{u}} = (\bar{\mathbf{u}}_l^m)_{l \geq 1}$ and

$$h_\varepsilon(\bar{\mathbf{u}}, x) = -u^{c,\varepsilon}(x) \quad \text{with} \quad u(z) = \sum_{l=0}^{\infty} \sum_{m=-l}^l \bar{\mathbf{u}}_l^m Y_l^m(z).$$

Note that the spherical harmonic coefficient $\bar{\mathbf{u}}_0^0$ equals 0 because of the identifiability condition $\int_{\mathbb{S}^2} u(x) d\mu_{\mathbb{S}^2}(x) = 0$.

We shall now discuss the equivalence between (4.4) and the original problem (4.1). On the 2-sphere, the series of spherical harmonics of a continuously differentiable function is uniformly convergent, see [44][p.259] or [43]. To obtain the stronger result that the sequence of spherical harmonics belongs to ℓ_1 , the function needs to be twice continuously differentiable, [43][Theorem 2]. For the unregularized potentials, such differentiability requires smoothness of the measures involved, as highlighted in Remark 3.1, but this holds for the regularized potential without any continuity condition for ν .

Proposition 4.1. *Let \mathbf{u}_ε be a solution of (4.1). Then, \mathbf{u}_ε is twice continuously differentiable, and, as a byproduct, its series of spherical harmonics belongs to ℓ_1 .*

The proof of the above result is detailed in our supplementary material. Consequently, the problem (4.4) is equivalent to the original one (4.1). The main virtue of this parameterization is that partial derivatives of h_ε with respect to the parameters $\bar{\mathbf{u}}_l^m$ can be derived easily, which is appealing in view of a stochastic gradient scheme. Here, the objective $h_\varepsilon(\cdot, x)$ is of the same mathematical nature than in [6], so that it is differentiable and the following property holds.

Proposition 4.2. *For every $x \in \mathbb{S}^2$, the function $h_\varepsilon(\cdot, x) : \ell_1 \rightarrow \mathbb{R}$ is Fréchet differentiable and its differential $D_{\bar{\mathbf{u}}}h_\varepsilon(\bar{\mathbf{u}}, x)$ belongs to the dual Banach space $(\ell_\infty, \|\cdot\|_{\ell_\infty})$ where $\|\bar{\mathbf{u}}\|_{\ell_\infty} = \sup_{l,m} |\bar{\mathbf{u}}_l^m|$. The components of $D_{\bar{\mathbf{u}}}h_\varepsilon(\bar{\mathbf{u}}, x)$ are the partial derivatives*

$$(4.5) \quad \frac{\partial h_\varepsilon(\bar{\mathbf{u}}, x)}{\partial \bar{\mathbf{u}}_l^m} = \frac{1}{4\pi} \int_{\mathbb{S}^2} g_{\bar{\mathbf{u}}, x}(z) Y_l^m(z) d\sigma_{\mathbb{S}^2}(z),$$

that are the spherical harmonics coefficients of the function

$$(4.6) \quad g_{\bar{\mathbf{u}}, x}(z) = \frac{\exp\left(\frac{u(z)-c(z,x)}{\varepsilon}\right)}{\int \exp\left(\frac{u(y)-c(y,x)}{\varepsilon}\right) d\mu_{\mathbb{S}^2}(y)} \quad \text{with} \quad u(z) = \sum_{l=0}^{\infty} \sum_{m=-l}^l \bar{\mathbf{u}}_l^m Y_l^m(z).$$

The algorithm. For (X_n) a sequence of independent random vectors with distribution ν , we consider the stochastic algorithm in the Banach space $(\ell_1, \|\cdot\|_{\ell_1})$ defined, for $n \geq 0$, by

$$(4.7) \quad \hat{\mathbf{u}}_{n+1} = \hat{\mathbf{u}}_n - \gamma_n W D_{\hat{\mathbf{u}}}h_\varepsilon(\hat{\mathbf{u}}_n, X_{n+1})$$

where $\gamma_n = \gamma n^{-\alpha}$ is a decreasing sequence of positive numbers with $1/2 < \alpha < 1$ and $\gamma > 0$. Because ℓ_1 differs from its dual space ℓ_∞ , the linear operator W is defined by

$$\begin{cases} W : (\ell_\infty, \|\cdot\|_{\ell_\infty}) & \rightarrow & (\ell_1, \|\cdot\|_{\ell_1}) \\ \bar{v} = (\bar{v}_l^m) & \mapsto & \bar{w} \odot \bar{v} = (\bar{w}_l^m \bar{v}_l^m) \end{cases}$$

where $\bar{w} = (\bar{w}_l^m)$ is a *deterministic sequence of positive weights* satisfying the condition

$$(4.8) \quad \|\bar{w}\|_{\ell_1} = \sum_{l=0}^{\infty} \sum_{m=-l}^l \bar{w}_l^m < +\infty.$$

In all the experiments carried out in this paper, we use $\bar{w}_l^m = (l^2 + m^2)^{-1}$. A *regularized estimator* of the optimal potential $\mathbf{u}_\varepsilon(x) = \sum_{l=0}^{\infty} \sum_{m=-l}^l \bar{\mathbf{u}}_{\varepsilon,l}^m Y_l^m(x)$ is naturally given by

$$(4.9) \quad \hat{\mathbf{u}}_{\varepsilon,n}(x) = \sum_{l=0}^{\infty} \sum_{m=-l}^l \hat{u}_{n,l}^m Y_l^m(x).$$

From a practical point of view, the stochastic sequence (4.7) must be discretized. To do so, one must consider a grid of p^2 points on the 2-sphere and the associated spherical harmonics coefficients. We emphasize that this discretization takes place in the space of frequencies, willing to take advantage from implicit interpolation in this space. The Python library *pyshtools* [84], implements spherical harmonics transforms and reconstructions. Our numerical procedure builds upon it as the stochastic algorithm (4.7) requires computing the spherical harmonics coefficients of the function $g_{\hat{u},y}(x)$ in (4.6), that relies on $u(x)$ reconstructed from \hat{u} thanks to the inverse Fourier transform on the 2-sphere. With the help of the fast routine within *pyshtools*, the computational cost at each iteration of (4.7) is of order $\mathcal{O}(p^2 \log^2(p))$.

Remark 4.1. *To study the convergence of the stochastic algorithm (4.7), we could adapt the theoretical results in [6] to our setting. Importantly, the convergence results (almost-sure convergence of estimators towards the minimizer in ℓ^2 -norm) obtained therein remain valid in the present spherical context, because they were irrespective of the orthonormal basis and the cost c . However, this is beyond the scope of this paper, that aims to showcase benefits of EOT for out-of-sample estimation.*

4.2. Regularized distribution and quantile functions. We now introduce the regularized counterpart of Definition 3.2. When dealing with measures supported on \mathbb{R}^d , one can use the *entropic map*, defined as the barycentric projection of the entropic optimal plan, [69]. At first sight, this requires a notion of average on the sphere, as done in [26] from the unregularized empirical OT plan. Nonetheless, this map is alternatively characterized by analogy with Brenier theorem [69], whose building block is the gradient of Kantorovich potential, as in [16] for OT with a general cost in \mathbb{R}^d . Because this enforces the structure of optimality, we pursue this idea for our non-Euclidean setting.

Definition 4.1. *Let ν be an arbitrary probability measure supported on \mathbb{S}^2 , and $\mathbf{u}_\varepsilon : \mathbb{S}^2 \rightarrow \mathbb{R}$ be a solution of (4.1) between $\mu_{\mathbb{S}^2}$ and ν . Then, the regularized distribution function of ν is given by*

$$(4.10) \quad \mathbf{F}_\varepsilon(z) = \text{Exp}_z(-\nabla \mathbf{u}_\varepsilon^{c,\varepsilon}(z)),$$

and the regularized quantile function of ν is

$$(4.11) \quad \mathbf{Q}_\varepsilon(x) = \text{Exp}_x(-\nabla \mathbf{u}_\varepsilon(x)).$$

This requires the differentiation of entropic Kantorovich potentials. For a given regularization parameter $\varepsilon > 0$, partial derivatives can be retrieved by

$$\frac{\partial \mathbf{u}_\varepsilon(x)}{\partial x_i} = \sum_{l=0}^{\infty} \sum_{m=-l}^l \bar{\mathbf{u}}_l^m \frac{\partial Y_l^m(x)}{\partial x_i},$$

where the package *sphericart* [8], allows the computation of $\frac{\partial Y_l^m(x)}{\partial x_i}$ easily. The Riemannian gradient $\nabla \mathbf{u}_\varepsilon$ follows using (3.7). But because this may lead to numerical instabilities, we suggest instead to make use of first-order conditions (4.3). Explicit forms for the generalized entropic maps on the hypersphere are given below. Their proof in the supplementary material follows by differentiating (4.3).

Proposition 4.3. *The regularized distribution and quantile functions of ν on \mathbb{S}^2 admit closed-form expressions through*

$$\mathbf{Q}_\varepsilon(x) = \text{Exp}_x \int \text{Log}_x(z) \exp\left(\frac{\mathbf{u}_\varepsilon(x) - c(x, z) + \mathbf{u}_\varepsilon^{c, \varepsilon}(z)}{\varepsilon}\right) d\nu(z),$$

and

$$\mathbf{F}_\varepsilon(z) = \text{Exp}_x \int \text{Log}_z(x) \exp\left(\frac{\mathbf{u}_\varepsilon(x) - c(x, z) + \mathbf{u}_\varepsilon^{c, \varepsilon}(z)}{\varepsilon}\right) d\mu_{\mathbb{S}^2}(x).$$

Remark 4.2. *We stress that \mathbf{F}_ε , resp. \mathbf{Q}_ε , does not push ν forward to $\mu_{\mathbb{S}^2}$ anymore, resp. $\mu_{\mathbb{S}^2}$ forward to ν . However, they are expected to be close to their unregularized counterparts, for small values of $\varepsilon > 0$, as studied, for the quadratic cost in \mathbb{R}^d , in [32, 69, 77]. The limit $\varepsilon \rightarrow 0$ has been studied outside the Euclidean setting [7, 64], although not directly about the generalized entropic map itself. In particular, up to some sequence (ε_k) such that $\lim_{k \rightarrow +\infty} \varepsilon_k = 0$, [64][Proposition 3.2] gives us the uniform convergence of potentials $(\mathbf{u}_{\varepsilon_k}, \mathbf{u}_{\varepsilon_k}^{c, \varepsilon_k})$ on compact subsets of \mathbb{S}^2 , towards (ψ, ψ^c) solving (3.10).*

From Proposition 4.3, \mathbf{F}_ε and \mathbf{Q}_ε can be seen as weighted averages in the tangent space. This can be gainful in practice, because of the regularity it induces. Indeed, second-order derivatives are given in our supplementary material, which entails continuity for \mathbf{F}_ε and \mathbf{Q}_ε . Finally, we stress that

$$(x, z) \mapsto \exp\left(\frac{\mathbf{u}_\varepsilon(x) - c(x, z) + \mathbf{u}_\varepsilon^{c, \varepsilon}(z)}{\varepsilon}\right)$$

is the density of the optimal entropic plan with respect to $\mu \otimes \nu$, [64]. Besides, by properties of exp and (4.3), it equals,

$$(4.12) \quad \frac{\exp\left(\frac{\mathbf{u}_\varepsilon(x) - c(x, z)}{\varepsilon}\right)}{\int \exp\left(\frac{\mathbf{u}_\varepsilon(y) - c(z, y)}{\varepsilon}\right) d\mu_{\mathbb{S}^2}(y)} = \frac{\exp\left(\frac{\mathbf{u}_\varepsilon^{c, \varepsilon}(z) - c(x, z)}{\varepsilon}\right)}{\int \exp\left(\frac{\mathbf{u}_\varepsilon^{c, \varepsilon}(y) - c(x, y)}{\varepsilon}\right) d\nu(y)}.$$

4.3. Regularized empirical distribution and quantile functions. Suppose that the estimator $\widehat{\mathbf{u}}_{\varepsilon,n}$, defined in (4.9), has been computed using the stochastic algorithm (4.7) from *i.i.d.* observations X_1, \dots, X_n sampled from ν supported on \mathbb{S}^2 . To obtain a regularized quantile function, the empirical counterpart of Proposition 4.3 would involve integrals with respect to $\mu_{\mathbb{S}^2}$ to compute the smooth conjugate of $\widehat{\mathbf{u}}_{\varepsilon,n}$. Therefore, to circumvent this issue, we consider a random sample U_1, \dots, U_N uniformly drawn on \mathbb{S}^2 , and we define the following estimator (as an approximation of $\widehat{\mathbf{u}}_{\varepsilon,n}^{c,\varepsilon}$)

$$(4.13) \quad \widehat{\mathbf{u}}_{N,n}^{c,\varepsilon}(z) = -\varepsilon \log \frac{1}{N} \sum_{i=1}^N \exp \left(\frac{\widehat{\mathbf{u}}_{\varepsilon,n}(U_i) - c(U_i, z)}{\varepsilon} \right).$$

Leveraging (4.12), we propose the following estimator, for the regularized quantile function \mathbf{Q}_ε defined in Proposition 4.3,

$$(4.14) \quad \widehat{\mathbf{Q}}_{N,n}^\varepsilon(x) = \text{Exp}_x \left(\sum_{i=1}^n \widehat{g}_{N,n}^\varepsilon(x, X_i) \text{Log}_x(X_i) \right),$$

where

$$\widehat{g}_{N,n}^\varepsilon(x, z) = \frac{\exp \left(\frac{\widehat{\mathbf{u}}_{N,n}^{c,\varepsilon}(z) - c(x, z)}{\varepsilon} \right)}{\sum_{j=1}^n \exp \left(\frac{\widehat{\mathbf{u}}_{N,n}^{c,\varepsilon}(X_j) - c(x, X_j)}{\varepsilon} \right)}.$$

In the same token, an estimator of \mathbf{F}_ε is given by

$$(4.15) \quad \widehat{\mathbf{F}}_{N,n}^\varepsilon(z) = \text{Exp}_z \left(\sum_{i=1}^N \widetilde{g}_{N,n}^\varepsilon(U_i, z) \text{Log}_z(U_i) \right),$$

with

$$\widetilde{g}_{N,n}^\varepsilon(x, z) = \frac{\exp \left(\frac{\widehat{\mathbf{u}}_{\varepsilon,n}(x) - c(x, z)}{\varepsilon} \right)}{\sum_{j=1}^N \exp \left(\frac{\widehat{\mathbf{u}}_{\varepsilon,n}(U_j) - c(U_j, z)}{\varepsilon} \right)}.$$

5. DEPTH-BASED DATA ANALYSIS

This section is dedicated to study a companion concept of directional MK quantiles, the MK statistical depth. We state a directional definition and discuss its properties. After that, we introduce descriptive tools in the spirit of the ones presented in [4, 51] in \mathbb{R}^d . For the sake of completeness, we first study the Euclidean setting \mathbb{R}^d before the directional one, that is of particular interest for us. Indeed, the results that we derive below do not appear as such in the literature, at least to the best of our knowledge.

5.1. Euclidean setting. We begin with the main definitions taken from [11]. Our chosen reference measure, denoted by U_d , is given by the random vector $R\Phi$, for R and Φ independently drawn from $[0, 1]$ and from the unit hypersphere $\mathbb{S}^{d-1} = \{\varphi \in \mathbb{R}^d : \|\varphi\| = 1\}$, respectively, as originally proposed in [11, 35] to define MK quantiles in \mathbb{R}^d . Note that the MK distribution function, the inverse of the MK quantile function, might not exist, *e.g.* if ν is discrete. Following [30], this is tackled with the Legendre-Fenchel dual of a convex function ψ , given by $\psi^*(x) = \sup_{u \in \mathbb{R}^d} \{ \langle x, u \rangle - \psi(u) \}$.

Definition 5.1 ([11]). *Let ν be a probability measure on \mathbb{R}^d . Its MK quantile function is the unique $\mathbf{Q} = \nabla\psi$ for some convex $\psi : \mathbb{R}^d \rightarrow \mathbb{R}$ such that $\mathbf{Q}_\#U_d = \nu$. Then, the MK α -quantile contour is $\mathbf{Q}(\{u \in \mathbb{R}^d : \|u\| = \alpha\})$. The sign curve associated to $u \in \mathbb{B}(0, 1)$ is $\mathbf{Q}(\{t \frac{u}{\|u\|} : t \in [0, 1]\})$. The MK depth of $x \in \mathbb{R}^d$ is the depth of $\nabla\psi^*$ under Tukey's depth, [78],*

$$D_\nu(x) = D_{U_d}^{Tukey}(\nabla\psi^*(x)).$$

The Liu-Zuo-Serfling axioms [50, 85], describe desirable properties for depth concepts. The MK-depth softens some of them, to reach more relevant contours [11]. Firstly, MK depth corresponds to Tukey depth for elliptical families [11]. Moreover, it benefits from invariance properties [30][Lemmas A.7, A.8], with respect to scaling (multiplication by a positive constant), translations, and orthogonal transformations (multiplication by an orthogonal matrix). Note that the affine-invariance does not hold. Another axiom is the *linear monotonicity relative to the deepest points*, that is $D_\nu(x) \leq D_\nu((1-t)x_0 + tx)$ for all $t \in [0, 1]$ if x_0 is a deepest point. This is not fulfilled by the MK depth [11], although it verifies a similar property along sign curves, as we shall see now.

Proposition 5.1 (Curvilinear monotonicity relative to the deepest points). *Assume that ν is continuous. The MK depth is monotonically decreasing along sign curves, that is, for each $u \in \mathbb{B}(0, 1)$ and $t \in [0, 1]$,*

$$D_\nu(\mathbf{Q}(u)) \leq D_\nu(\mathbf{Q}(tu)).$$

Proof. Recall that Tukey's depth verifies linear monotonicity relative to the deepest points [85]. As the origin is the deepest point for U_d , this writes, for any $t \in [0, 1]$,

$$(5.1) \quad D_{U_d}^{Tukey}(u) \leq D_{U_d}^{Tukey}(tu).$$

From Definition 5.1, $D_\nu(\mathbf{Q}(u)) = D_{U_d}^{Tukey}(\nabla\psi^* \circ \mathbf{Q}(u))$. By continuity of ν , $\nabla\psi^* \circ \mathbf{Q}(u) = u$ *a.e.*, [80][Theorem 2.12 and Corollary 2.3]. Thus the result follows, with (5.1). \square

This corresponds to the classical linear monotonicity under distributions with straight sign curves, including spherical families due to the particular form of the MK quantile function in this setting, taken from [11].

Corollary 5.1. *For spherically symmetric distributions, sign curves are straight lines, and the MK depth verifies linear monotonicity relative to the deepest point. For any x in the support of ν , for m the MK deepest point of ν ,*

$$(5.2) \quad \forall t \in [0, 1], D_\nu(x) \leq D_\nu((1-t)m + tx).$$

Proof. Let X be a random vector associated with a spherically symmetric distribution. By inverting the MK distribution function known from [11],

$$\mathbf{Q}(u) = \frac{u}{\|u\|} G^{-1}(\|u\|) + m,$$

where G is the univariate distribution function of the radial part $\|X - m\|$. Because $\|X\| \geq 0$ a.s. and G^{-1} is increasing, $G^{-1}(t\|u\|)/G^{-1}(\|u\|) \in [0, 1]$ and

$$\mathbf{Q}(tu) = \frac{u}{\|u\|} G^{-1}(t\|u\|) + m = \frac{G^{-1}(t\|u\|)}{G^{-1}(\|u\|)} (\mathbf{Q}(u) - m) + m.$$

This rewrites, for $\delta_t = G^{-1}(t\|u\|)/G^{-1}(\|u\|)$, $\mathbf{Q}(tu) = \delta_t \mathbf{Q}(u) + (1 - \delta_t)m$. Besides, δ_t takes all values between 0 and 1 for $t \in [0, 1]$. This, combined with Proposition 5.1 induces

$$\forall u \in \mathbb{B}(0, 1), \forall \delta \in [0, 1], D_\nu(\mathbf{Q}(u)) \leq D_\nu(\delta \mathbf{Q}(u) + (1 - \delta)m).$$

But any x in the support of ν writes $\mathbf{Q}(u)$ for $u = \mathbf{F}(x)$, which gives (5.2). \square

5.2. Directional setting. Using the same ideas, one can define the MK depth on the sphere through any statistical depth with respect to the uniform $\mu_{\mathbb{S}^2}$ oriented towards $\mathbf{F}(\theta_M)$, and the simplest is surely to consider the proximity with $\mathbf{F}(\theta_M)$.

Definition 5.2. *Let ν be an arbitrary probability measure on \mathbb{S}^2 , with directional distribution function \mathbf{F} . The directional MK depth of $x \in \mathbb{S}^2$ is defined by $D_\nu(x) = 1 - d(\mathbf{F}(x), \mathbf{F}(\theta_M))/\pi$.*

Regarding the \mathbb{S}^2 -adapted versions of Liu-Zuo-Serfling axioms, [50, 85], the directional MK depth behaves like its Euclidean counterpart. We begin with the four classical properties which are analogs of the Euclidean axioms, [47]. The affine-invariance is replaced on \mathbb{S}^2 by rotational invariance, which holds true from the supplementary material of [37]. Moreover, it is straightforward that D_ν attains its maximum at the center θ_M , and that it vanishes at x such that $\mathbf{F}(x) = -\mathbf{F}(\theta_M)$. Hence, outliers outside the support of the distribution will be ranked around $-\mathbf{F}(\theta_M)$ and will have vanishing depth. Finally, monotonicity along great circles is not fulfilled, but it is replaced in the same data-adaptive fashion than in \mathbb{R}^d .

Proposition 5.2 (Curvilinear monotonicity relative to the deepest points). *Assume that ν is continuous. The directional MK depth is monotonically decreasing along sign curves. For each $x \in \mathbb{S}^2$ and $t \in [\langle x, \mathbf{F}(\theta_M) \rangle, 1]$, let $x_t \in \mathcal{M}_s^U$, for $s = \mathbf{S}_{\mathbf{F}(\theta_M)}(x)$, such that*

$$(5.3) \quad x_t = t\mathbf{F}(\theta_M) + \sqrt{1 - t^2}s.$$

Then,

$$D_\nu(\mathbf{Q}(x)) \leq D_\nu(\mathbf{Q}(x_t)).$$

Proof. Fix $x \in \mathbb{S}^2$. From the decomposition (3.12), $s = \mathbf{S}_{\mathbf{F}(\theta_M)}(x)$ is the directional sign associated to x . For $t \in [-1, 1]$, let $x_t \in \mathcal{M}_s^U$ be a parameterization of the reference sign curve associated to s , as in (5.3). Immediately, one may note that $\langle x_t, \mathbf{F}(\theta_M) \rangle = t$, and $x_t = x$ for $t = \langle x, \mathbf{F}(\theta_M) \rangle$. Besides, $D_\nu(\mathbf{Q}(x_t)) = 1 - d(x_t, \mathbf{F}(\theta_M))/\pi = 1 - \arccos(t)/\pi$, so, as soon as $t \geq \langle x, \mathbf{F}(\theta_M) \rangle$, $D_\nu(\mathbf{Q}(x_t)) \geq D_\nu(\mathbf{Q}(x))$. \square

Explicit formulations for rotationally invariant distributions are given in [37], and recalled in the supplementary material, so that the following is straightforward.

Corollary 5.2. *For rotationally invariant distributions, sign curves are great circles. Thus, the MK depth verifies linear monotonicity along great circles, relative to the deepest point.*

Proof. Without loss of generality, assume that $\theta_M = (0, 0, 1)^T$, which can always be ensured by applying a rotation to the data. Then, from the supplementary of [37], $x \in \mathbb{S}^2$ and $\mathbf{Q}(x)$ only differ from their latitude, under the assumption of ν to be rotationally invariant. Thus, sign curves are great circles, and the result follows. \square

Other desirable axioms have been put forward recently in [61, 62], namely the *upper semi-continuity* and the *non-rigidity of central regions*. *Upper semi-continuity* is ensured as soon as the MK distribution function \mathbf{F} is continuous, thus at least for $\nu \in \mathbf{B}_2$. When ν is arbitrary, taking the regularized directional MK depth built from \mathbf{F}_ε , for $\varepsilon > 0$, imposes continuity. The *non-rigidity of central regions* states that quantile regions are not restricted to be spherical caps, which is readily true for the MK depth. In fact, its adaptivity to the underlying support can be seen as a stronger *non-rigidity* axiom, requiring that $\mathbf{Q}(U) \sim \nu$ as soon as $U \sim \mu$. Furthermore, Proposition 5.2 and Corollary 5.2 shed some light on the non-verified axiom of *monotony along great circles*. Our results suggest that the directional MK depth alleviates these axioms when necessary, for complex distributions such as mixtures, whereas the axioms are fulfilled for distributions for which it is useful, in particular for rotationally invariant ones.

6. NUMERICAL EXPERIMENTS

6.1. Choice of ε and comparison of EOT and OT. The calibration of ε is a common issue in EOT. It can be selected by cross-validation, as with any hyper-parameter, or it can be selected with a transport-based criterion [79]. In this section, we shall see that $\varepsilon \approx 0.1$ leads to accurate results overall, leading to this choice as a baseline in all the experiments of this paper.

6.1.1. *Quantitative effect of regularization.* In Figure 1, we study the influence of the regularization parameter on a quantitative metric: we compare against ground-truth contours of the isotropic von-Mises Fisher distribution. Indeed, this is the only distribution for which explicit formula are known. This was first established by [37] and it is recalled in the supplementary material for the sake of completeness. The mean-squared error from uniform samples $(x_i) \subset \mathbb{S}^2$ is

$$\mathcal{R}_n(\widehat{Q}) = \frac{1}{n} \sum_{i=1}^n c(Q(x_i), \widehat{Q}(x_i)),$$

for \widehat{Q} denoting either our regularized MK quantile estimator or the unregularized one proposed in [37]. Estimators \widehat{Q} are evaluated on samples of size $n = 500$ drawn from the uniform $\mu_{\mathbb{S}^2}$ and from a von-Mises fisher distribution of location $(0, 0, 1)^T$ and concentration $\kappa = 10$. By doing this experiment 100 times, we obtain a boxplot of MSE values for various values of ε . The results are reported in Figure 1, where $\varepsilon = 0$ refers to the MSE of \widehat{Q}_0 . The dashed horizontal line illustrates the median value for the MSE of \widehat{Q}_0 . It can be observed that entropic regularization is able to significantly outperform the estimation of the quantile map, in particular for values around $\varepsilon \approx 0.1$. Increasing the sample size leads to similar conclusions.

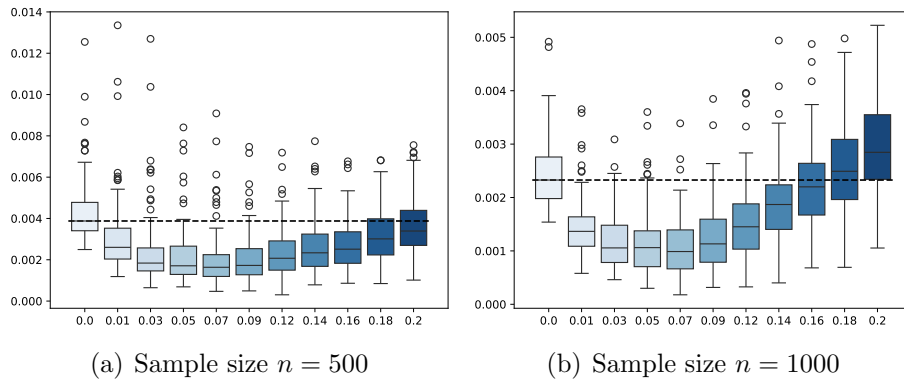


Figure 1. Mean squared error $\mathcal{R}_n(\widehat{Q}_\varepsilon)$ as a function of the regularization parameter $\varepsilon \in [0, 0.2]$. The horizontal dashed-line is the value of $\mathcal{R}_n(\widehat{Q}_0)$.

6.1.2. *Qualitative effect of regularization.* In Figure 2, we visually compare regularized and unregularized MK spherical quantile contours of orders 24.4%, 48.8%, 75.6% on the same von-Mises fisher distribution than in Figure 1. Such uncommon probability contents are inherent to unregularized contours because the number of contours (and their size) depends on a fixed grid, and a fortiori on the sample size, that is here fixed at $n = 2001$. Ground-truth contours are presented together with unregularized and regularized ones, for $\varepsilon \in \{0.01, 0.05, 1\}$. Each contour contains 100 points,

linked by straight lines. For $\varepsilon = 0.01$, contours adapt too much on the finite-sample data, causing errors as ground-truth contours are smoother. For $\varepsilon = 1$, contours are smoother, but there is too much bias in the approximation between $\widehat{\mathbf{Q}}_\varepsilon$ and the underlying ground truth. For the well-chosen $\varepsilon = 0.05$, the trade-off between regularity and low-bias allows the better estimation. This sheds some light on the behavior of regularization. The lower the ε , the more adapted $\widehat{\mathbf{Q}}_\varepsilon$ is to the finite-sample data and its irregularities. Larger values of ε induce smoother contours, as a byproduct of a greater regularity for $\widehat{\mathbf{Q}}_\varepsilon$.

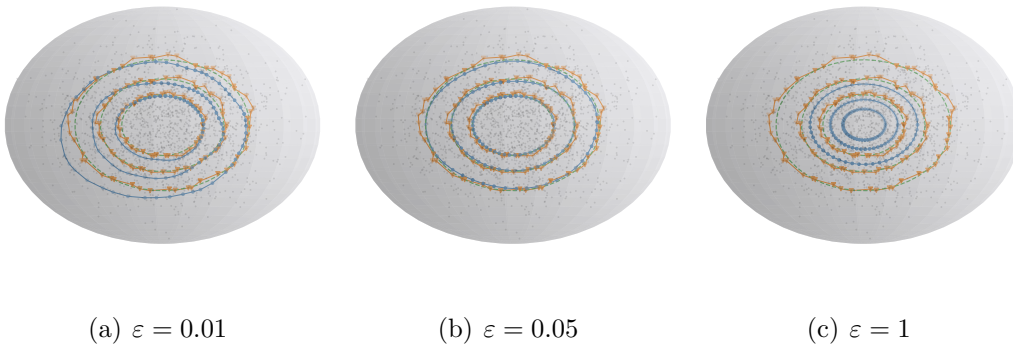


Figure 2. Empirical regularized quantile contours (blue dots), unregularized ones (orange triangles), and ground truth (dashed green line).

6.1.3. *Structural differences between regularized and unregularized estimation.* The estimation of contours in [37] involves a matching between two samples of same size, hence it is not a functional object, in contrast to our entropic estimator.

Two versus one OT problem. Firstly, we stress that the estimation of contours in [37] requires to solve two different OT problems. The construction of a uniform grid requires the choice of a reference central point (there is no origin on the sphere). Thus, a first OT problem estimates this central point $\mathbf{F}(\theta_M)$ from the Fréchet median θ_M , and a second one involves a grid (the reference contours) oriented towards the estimate of $\mathbf{F}(\theta_M)$. This is not at all the case with our algorithm for which the estimate $\widehat{\mathbf{u}}_{\varepsilon,n}$ yields directly $\widehat{\mathbf{F}}_{N,n}^\varepsilon$ and $\widehat{\mathbf{Q}}_{N,n}^\varepsilon$, and a fortiori $\widehat{\mathbf{F}}_{N,n}^\varepsilon(\theta_M)$. Reference contours are then oriented to the central point $\widehat{\mathbf{F}}_{N,n}^\varepsilon(\theta_M)$, and their image by $\widehat{\mathbf{Q}}_{N,n}^\varepsilon$ yields quantile contours without the need to solve an additional OT problem. The time to compute a single OT/EOT problem is reported in Figure 3, where it is shown that our algorithm is mostly profitable for large sample sizes.

Out-of-sample estimation. Figure 4 illustrates MK quantile contours on a mixture of von-Mises Fisher distributions, with $\varepsilon = 0.1$. Because unregularized quantiles involve a bijection between the reference grid and the data, it is not able to compute

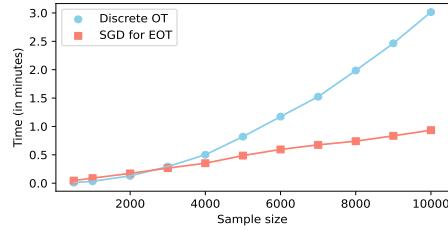


Figure 3. Time for solving regularized and unregularized optimal transport between two data with n instances, as a function of n .

the MK depth on points outside of the data. On the contrary, our entropic estimator $\hat{\mathbf{F}}_{N,n}^\epsilon$ can be computed at any $x \in \mathbb{S}^{d-1}$, allowing to evaluate the MK depth at any out-of-sample observation. The upcoming numerical experiments illustrate how this specific property of our estimator is needed for descriptive analysis and depth-based classification.

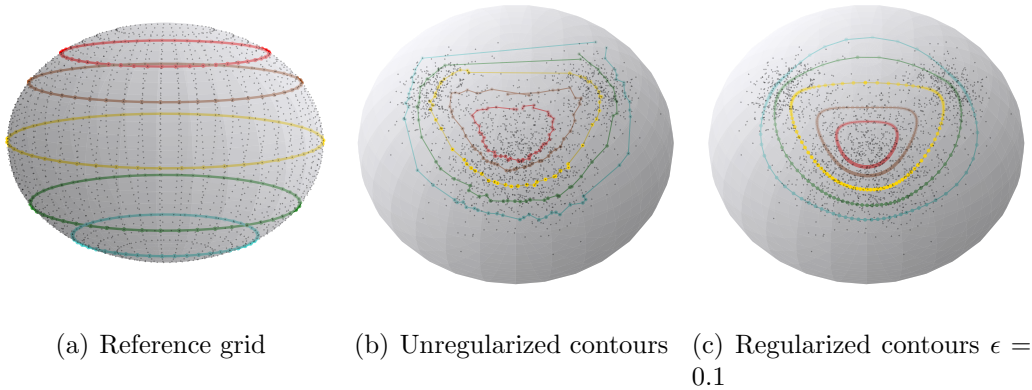


Figure 4. Empirical MK quantile contours on a mixture of vMF distributions

6.2. Descriptive tools. The seminal paper [51] gathers descriptive tools based on data depths. Monge-Kantorovich analogs already exist for data in \mathbb{R}^d , and we shall now extend some of them to the directional setting. We stress that the ability of our regularized estimator to interpolate between data points is crucial for (i) smooth contours in practice and (ii) computing volumes of quantile regions.

6.2.1. Representative plots. Firstly, [51] study representative plots for bivariate data, and the MK analog is given by the descriptive plots from [35, 37], the latter with the added information of sign curves. Figure 5 illustrates it on a Tangent von-Mises Fisher distribution, [27], and on a Mixture of two von-Mises Fisher distributions, with the help of our empirical regularized quantile function. One can observe that

the shapes of the distributions are well recovered. Because entropic MK quantiles interpolate between data points, contours cross the void between mixture components on the right-hand side. A careful inspection shows that the number of points per contour within this void is much lower than in the high density areas. This illustrates how the variation of mass, that is the underlying geometry, is captured by our regularized estimator.

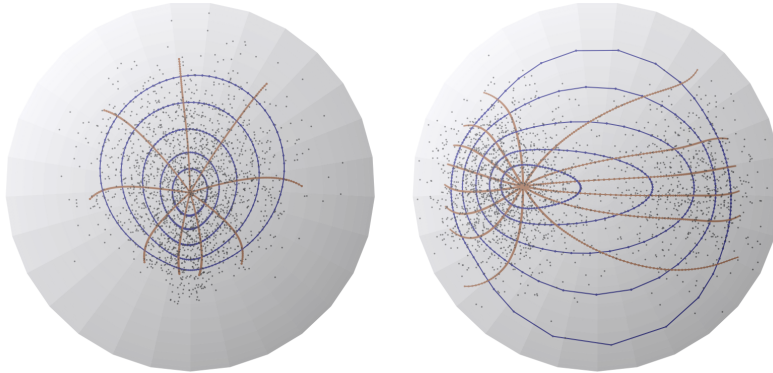


Figure 5. Regularized quantile contours of levels $\{0.1, 0.25, 0.5, 0.75, 0.9\}$ and associated sign curves, with $\epsilon = 0.1$.

6.2.2. *Scale or dispersion.* We now present a graphical tool to describe the amount of dispersion, called the *scale curve* in [51] and whose MK analog has been introduced in [4] for Euclidean data. The *scale curve* is a plot of the volumes $V(\alpha)$ of MK quantile regions with respect to $\alpha \in [0, 1]$. The faster it grows, the greater the dispersion. Thus, if the scale curve of ν_1 is consistently above the one of ν_2 , then ν_1 is more spread out than ν_2 . Define

$$V(\alpha) = \int_{\mathbb{C}_\alpha} d\mu_{\mathbb{S}^2}(x) = \int_{\mathbb{S}^2} \mathbf{1}_{\{x \in \mathbb{C}_\alpha\}} d\mu_{\mathbb{S}^2}(x) = \int_{\mathbb{S}^2} \mathbf{1}_{\{\langle \mathbf{F}(x), \mathbf{F}(\theta_M) \rangle \geq 1-2\alpha\}} d\mu_{\mathbb{S}^2}(x).$$

This can be estimated with a sample U_1, \dots, U_N from $\mu_{\mathbb{S}^2}$, by the proportion $V_{\epsilon, n}(\alpha) = \frac{1}{N} \sum_{i=1}^N \mathbf{1}_{\{\langle \hat{\mathbf{F}}_{N, n}^\epsilon(U_i), \mathbf{F}(\theta_M) \rangle \geq 1-2\alpha\}}$. Crucially, this requires to estimate $\mathbf{F}(x)$ for out-of-sample observations x , for which regularization is needed. On the left-hand side of Figure 6, we draw the scale curves of von-Mises Fisher distributions with varying concentration parameter $\kappa \in \{1, 2, 5, 15\}$, which controls the dispersion of samples. It is well-captured that the lower the value of κ , the more spread out is the underlying distribution. We also illustrate in the right-hand side of Figure 6 that the scale curve captures the presence of outliers. We consider three identical vMF distributions with dispersion parameter $\kappa = 15$ and mean $(0, 1, 0)^T$. Adding $N \in \{5, 20, 50\}$ outliers near from the North Pole $(0, 0, 1)^T$, the dispersion increases with the number of outliers, which is precisely the expected behavior.

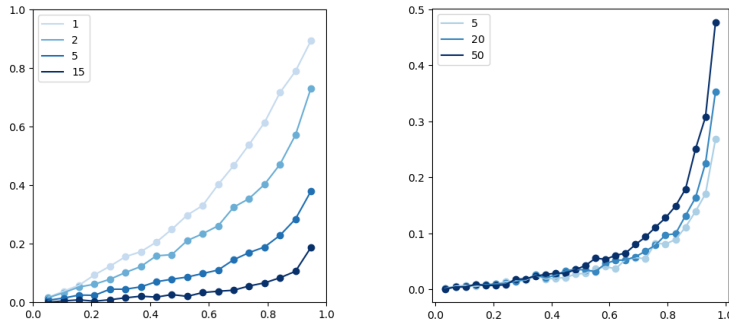


Figure 6. Scale curves of von-Mises Fisher distributions with various (left) dispersion parameter κ and (right) number N of added outliers.

6.3. Other concepts of quantiles. In Figure 7, we display a visual comparison of existing concepts for quantiles on the sphere by focusing on mixtures of von-Mises Fisher distributions. All distributions are centered for ease of visualization with azimuth angle 90 degrees and elevation angle 5 degrees. It can be observed from Figure 7 that Mahalanobis quantile regions [47] are concentric spherical caps, whereas spatial quantiles [45] and our regularized MK quantiles can exhibit more complex shapes that better fit the geometry of the data. To that extent, spatial and regularized MK quantiles, are both more satisfactory. For each notion of quantiles, 100 points are drawn within each contours, with straight lines to link them. We emphasize that spatial quantiles are not indexed by their probability content, as opposed to the MK ones [37].

6.4. Max-depth classification. Following experiments in [45], we report a *quantitative comparison* between different notions of directional quantiles on the task of supervised classification, based on the *max-depth* approach from [31]. Because statistical depths are designed to measure *outlyingness* within a distribution, one can classify $x \in \mathbb{S}^2$ as coming from the distribution ν_1 instead of ν_2 if the depth of x with respect to (*w.r.t.*) ν_1 is greater than the one *w.r.t.* ν_2 . As highlighted in [45], the vanishing property of many statistical depths [52, 78], raises issues when the sample x lies outside the convex hull of empirical data, where new data is classified randomly. On the contrary, the depth associated to spatial quantiles [45][Section 5], is strictly positive everywhere, and the same holds trivially for the MK depth. The regularization parameter for EOT is taken as $\varepsilon = 10^{-1}$. Define O the rotation matrix fixing the first coordinate and mapping $m_1 = (0, 0, 1)^T$ to $m_2 = (0, \sin(\pi/3), \cos(\pi/3))^T$. We consider for (P_1, P_2) :

- (1) *von-Mises Fisher*: P_1 is a vMF with location m_1 and concentration $\kappa = 3$, P_2 is the distribution of OX for $X \sim P_1$.

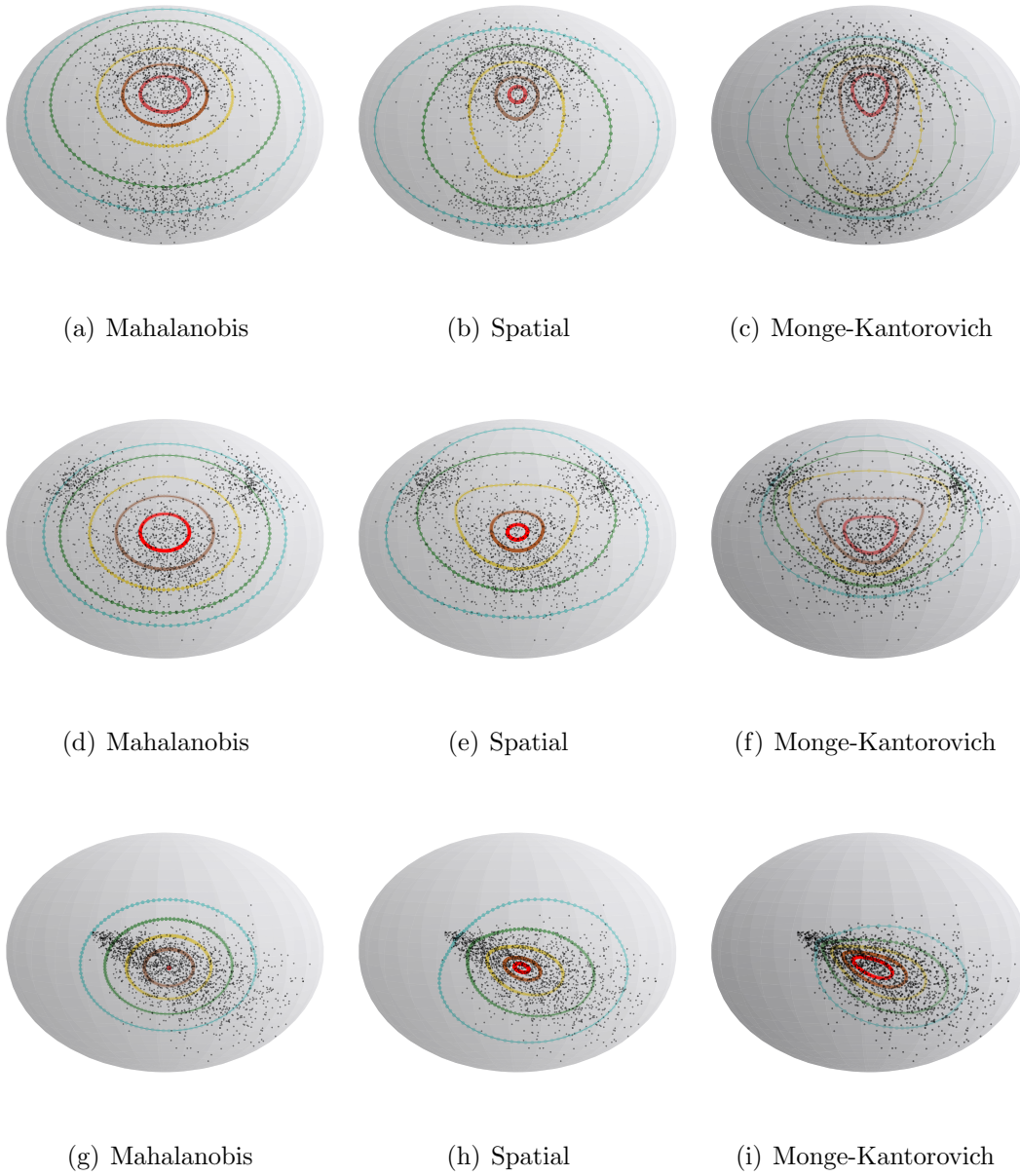


Figure 7. Quantile contours $\{0.1, 0.25, 0.5, 0.75, 0.9\}$ for different definitions of quantiles and data sampled from mixtures of two (first row) and three (second row) von-Mises Fisher distributions, and from a Tangent vMF (third row).

(2) *Tangent von-Mises Fisher*: P_1 is the distribution of

$$X = Zm_1 + \sqrt{1 - Z^2}S,$$

where $Z = 2V - 1$ for V a Beta(2, 8) distribution, $S_3 = 0$ and $(S_1, S_2)^T$ follows a von-Mises Fisher distribution with location $(1, 0)^T$ and concentration $\kappa' = 5$. Again, P_2 is the distribution of OX for $X \sim P_1$.

(3) *Non-convex data* : P_1 is the same mixture of three vMF distributions than in Figure 7. P_2 is a vMF distribution centered at $(0, 0, 1)^T$ with concentration parameter $\kappa = 50$.

Examples of data sampled from these three distributions are displayed in Figure 8, with observations sampled from P_1 in blue and P_2 in red.

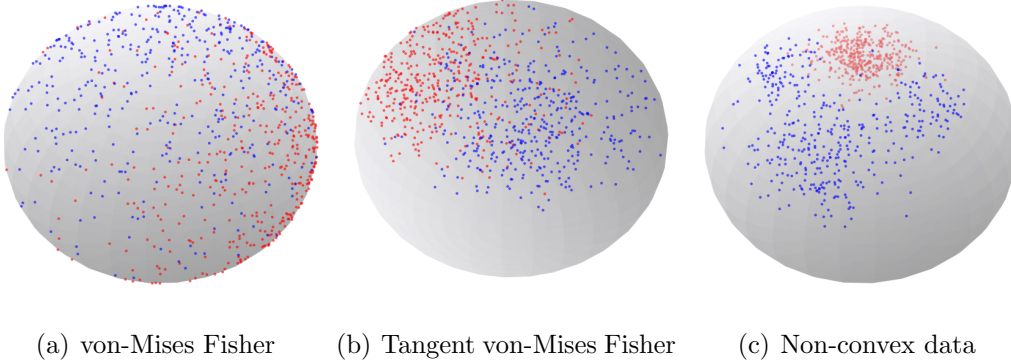


Figure 8. Data for max-depth classification.

In each setting, we learn the quantile functions on 200 points coming from distributions (P_1, P_2) , before computing misclassification rates on a test data of 200 different observations. This is repeated 100 times and the misclassification rates are gathered in Figure 9. All methods provide comparative results when both the supports of P_1 and P_2 are convex. However, in the third setting, classification based on the MK depth significantly outperforms the others. This illustrates the potential of entropically regularized quantiles for statistical purposes.

These results are complemented in Figure 10 with misclassification rates of the MK depth in the non-convex setting, but changing the regularization parameter. This highlights that other values of ϵ lead to even better classification results. Thus, beyond the convenient baseline of $\epsilon = 0.1$ that performs well overall, one may consider cross-validation of ϵ if enough data is available. Figure 10 also contains further comparison between depth notions in the non-convex setting and with $\epsilon = 0.1$. There, the training and testing subsets have a larger sample size, either $n = 500$ or $n = 1000$. This validates results from Figure 9.

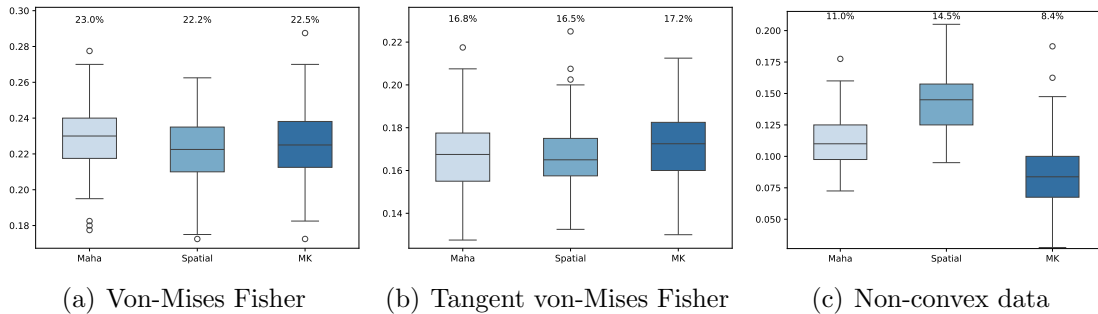


Figure 9. Misclassification rates with several statistical depths.

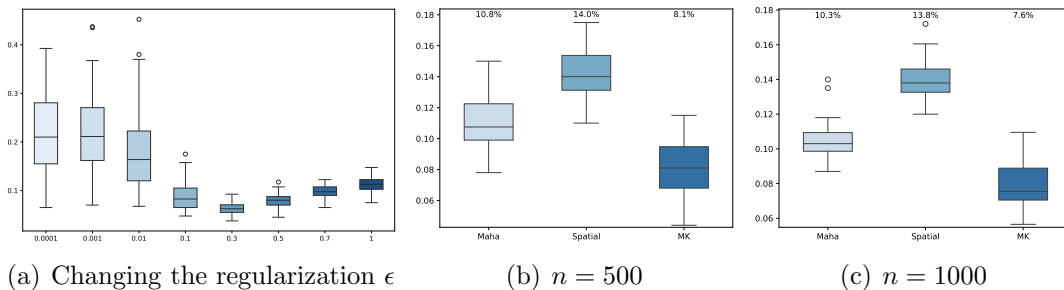


Figure 10. Further misclassification rates in the non-convex setting, with various ϵ values and for larger sample size.

7. CONCLUDING REMARKS

The major limitation of discrete OT for quantiles estimation is the impossibility to provide out-of-sample estimates $Q(x)$ that interpolate the data. In the present paper, we showed that regularizing by entropy can be used as an alternative, particularly when the focus is on the quantile contours or the volumes of quantile regions. Still, we emphasize that this regularization loses the distribution-freeness of the ranks, which is crucial for testing purposes, [37]. Thus, the choice of using OT or EOT shall depend on the considered task.

Our numerical scheme leverages spherical Fourier series to construct a stochastic gradient descent to solve *continuous* OT in the limit of the iterations. This is particularly useful when the number of observations n is large and/or when data arrives sequentially. A natural perspective would be to extend these results to other manifolds, in light with the recent work [36], or to the statistics of circular data, discussed in detail in [42]. The main limitation of the present work concerns the dimensionality, even though most applications in directional statistics has been implemented in dimension $d = 3$. This is inherited from the computation of spherical harmonics, since we use the Python library *pyshtools* [84]. However, our implementation could in principle be extended to $d > 3$ from other spherical harmonics transforms.

APPENDIX

The supplementary material gathers detailed proofs for all the results related to the differentiation of entropic maps and potentials. It also describes how the explicit forms of spherical MK quantiles from [37] are computed in our numerical experiments, as they simplify in dimension $d = 3$.

APPENDIX A. EXPLICIT FORMS

Closed-form expressions of \mathbf{F} for rotationally invariant distributions were given in [37] allowing to deduce the inverse map \mathbf{Q} . Because part of our numerical experiments rely on these, this section gathers such explicit forms, as they simplify in dimension $d = 3$.

Let $Z \sim \nu$ be such a random vector with axis $\pm\theta_M$. Then, assume that ν has density

$$z \in \mathbb{S}^2 \mapsto c_f f(z^T \theta_M),$$

for f some positive *angular function* and c_f a normalizing constant. For $r \in [-1, 1]$, denote by

$$F_f(r) = \int_{-1}^r f(s) ds / \int_{-1}^1 f(s) ds$$

the distribution function of $Z^T \theta_M$ and by $Q_f = F_f^{-1}$ its quantile function. Then, letting $F_f^*(r) = 2F_f(r) - 1$, the directional distribution function of Z writes

$$(A.1) \quad \mathbf{F}(z) = F_f^*(z^T \theta_M) \theta_M + \sqrt{1 - F_f^*(z^T \theta_M)^2} S_{\theta_M}(z).$$

For instance, taking $f(s) = \exp(\kappa z^T \theta_M)$ corresponds to the von Mises-Fisher distribution with location parameter θ_M and concentration parameter $\kappa \in \mathbb{R}_+$. Crucially, the transport (A.1) reduces to univariate transport along the axis $\theta_M = \mathbf{F}(\theta_M)$. If $\theta_M = (0, 0, 1)^T$, that is to say *up to some rotation* thanks to equivariance properties shown in [37], this corresponds to changing the latitude *w.r.t.* the usual coordinate system

$$(A.2) \quad x = \Phi(\theta, \phi) := (\cos \phi \sin \theta, \sin \phi \sin \theta, \cos \theta).$$

Indeed, as soon as $\theta_M = (0, 0, 1)^T$,

$$\mathbf{F}(z) = F_f^*(z_3) \theta_M + \sqrt{1 - F_f^*(z_3)^2} \frac{(z_1, z_2, 0)^T}{\|(z_1, z_2, 0)^T\|}.$$

The third coordinate is changed to $F_f^*(z_3)$, and the other coordinates are adapted to the constraint $\mathbf{F}(z) \in \mathbb{S}^2$. This rewrites, in accordance with (A.2),

$$(A.3) \quad \mathbf{F}(z) = \mathbf{F}(\Phi(\theta, \phi)) = \Phi(\bar{\theta}, \phi) \quad \text{for} \quad \bar{\theta} = \arccos \left((F_f^*)(z_3) \right).$$

Consequently, to get the inverse map $\mathbf{Q} = \mathbf{F}^{-1}$, it suffices to change the pseudo latitude of $\mathbf{F}(z) \in \mathcal{C}_\tau^U$ w.r.t. the axis $\pm\theta_M$. If $x = \mathbf{F}(z)$, $x_3 = F_f^*(z_3)$ and $z_3 = (F_f^*)^{-1}(x_3)$, that is

$$(A.4) \quad \mathbf{Q}(x) = \mathbf{Q}(\Phi(\theta, \phi)) = \Phi(\tilde{\theta}, \phi) \quad \text{for} \quad \tilde{\theta} = \arccos\left((F_f^*)^{-1}(x_3)\right).$$

As highlighted in [37], this shows that MK quantile contours coincide with Mahalanobis ones from [47] under the rotationally symmetric model.

APPENDIX B. FIRST-ORDER DIFFERENTIATION OF ENTROPIC POTENTIALS

This section is dedicated to the proof of Proposition 4.3, that gives explicit spherical entropic maps.

B.1. Euclidean derivatives.

Proposition B.1. *Denote by*

$$(B.1) \quad g_\varepsilon(x, z) = \frac{-d(x, z)}{\sqrt{1 - \langle x, z \rangle^2}} \exp\left(\frac{\mathbf{u}_\varepsilon(x) - c(x, z) + \mathbf{u}_\varepsilon^{c, \varepsilon}(z)}{\varepsilon}\right).$$

Then, the Euclidean partial derivatives of \mathbf{u}_ε admit the closed-form expression

$$(B.2) \quad \partial_{x_i} \mathbf{u}_\varepsilon(x) = \int z_i g_\varepsilon(x, z) d\nu(z).$$

Similarly, the Euclidean gradient of $\mathbf{u}_\varepsilon^{c, \varepsilon}$ verifies

$$(B.3) \quad \partial_{z_i} \mathbf{u}_\varepsilon^{c, \varepsilon}(z) = \int x_i g_\varepsilon(x, z) d\mu_{\mathbb{S}^2}(x).$$

Denoting by $v = \mathbf{u}_\varepsilon^{c, \varepsilon}$, rewriting the optimality condition $\mathbf{u}_\varepsilon = (\mathbf{u}_\varepsilon^{c, \varepsilon})^{c, \varepsilon}$ gives

$$\mathbf{u}_\varepsilon(x) = -\varepsilon \log \int \exp\left(\frac{v(z) - c(x, z)}{\varepsilon}\right) d\nu(z).$$

By the chain rule,

$$(B.4) \quad \partial_{x_i} \mathbf{u}_\varepsilon(x) = -\varepsilon \frac{\partial_{x_i} J(x)}{J(x)} \quad \text{for} \quad J(x) = \int \exp\left(\frac{v(z) - c(x, z)}{\varepsilon}\right) d\nu(z).$$

We now turn to the differentiation of J . As shown in [64][Lemma 2.1],

$$\inf_{x \in \mathbb{S}^2} \{c(x, z) - \mathbf{u}_\varepsilon(x)\} \leq v(z) \leq \int c(x, z) d\mu_{\mathbb{S}^2}(x).$$

By boundedness of \mathbb{S}^2 , v is bounded and so is the integrand in (B.4). As we deal with probability measures, this justifies using the differentiation under the integral sign, that is

$$\partial_{x_i} J(x) = \int \partial_{x_i} \exp\left(\frac{v(z) - c(x, z)}{\varepsilon}\right) d\nu(z),$$

which induces

$$(B.5) \quad \partial_{x_i} J(x) = \int -\frac{\partial_{x_i} c(x, z)}{\varepsilon} \exp\left(\frac{v(z) - c(x, z)}{\varepsilon}\right) d\nu(z).$$

Fix $z \in \mathbb{S}^2$, so

$$(B.6) \quad \partial_{x_i} c(x, z) = d(x, z) \partial_{x_i} d(x, z) \quad \text{and} \quad \partial_{x_i} d(x, z) = \frac{-1}{\sqrt{1 - \langle x, z \rangle^2}} z_i.$$

Combining (B.5) with (B.6),

$$(B.7) \quad \partial_{x_i} J(x) = \int \frac{z_i}{\varepsilon} \frac{d(x, z)}{\sqrt{1 - \langle x, z \rangle^2}} \exp\left(\frac{v(z) - c(x, z)}{\varepsilon}\right) d\nu(z).$$

Plugging (B.7) in (B.4) gives (B.3), where g_ε defined in (B.1) shows up because

$$(B.8) \quad \exp\left(\frac{\mathbf{u}_\varepsilon(x) - c(x, z) + \mathbf{u}_\varepsilon^{c, \varepsilon}(z)}{\varepsilon}\right) = \frac{\exp\left(\frac{\mathbf{u}_\varepsilon^{c, \varepsilon}(z) - c(x, z)}{\varepsilon}\right)}{\int \exp\left(\frac{\mathbf{u}_\varepsilon^{c, \varepsilon}(y) - c(x, y)}{\varepsilon}\right) d\nu(y)}.$$

The same arguments on $\mathbf{u}_\varepsilon^{c, \varepsilon}(z)$ yield (B.2). \square

B.2. Proof of Proposition 4.3. Using the Euclidean derivatives obtained in Proposition B.1,

$$\nabla \mathbf{u}_\varepsilon(x) = \rho_x \int z g_\varepsilon(x, z) d\nu(z) \quad \text{and} \quad \nabla \mathbf{u}_\varepsilon^{c, \varepsilon}(z) = \rho_z \int x g_\varepsilon(x, z) d\mu_{\mathbb{S}^2}(x).$$

But this is equivalent to

$$\nabla \mathbf{u}_\varepsilon(x) = \int -\frac{d(x, z)}{\sqrt{1 - \langle x, z \rangle^2}} \rho_x(z) \exp\left(\frac{\mathbf{u}_\varepsilon(x) - c(x, z) + \mathbf{u}_\varepsilon^{c, \varepsilon}(z)}{\varepsilon}\right) d\nu(z),$$

and

$$\nabla \mathbf{u}_\varepsilon^{c, \varepsilon}(z) = \int -\frac{d(x, z)}{\sqrt{1 - \langle x, z \rangle^2}} \rho_z(x) \exp\left(\frac{\mathbf{u}_\varepsilon(x) - c(x, z) + \mathbf{u}_\varepsilon^{c, \varepsilon}(z)}{\varepsilon}\right) d\mu_{\mathbb{S}^2}(x).$$

There, one recovers $\text{Log}_x = \text{Exp}_x^{-1}$ as in

$$(B.9) \quad \text{Log}_x(z) = \frac{d(x, z)}{\sqrt{1 - \langle x, z \rangle^2}} \rho_x z = d(x, z) \frac{\rho_x(z - x)}{\|\rho_x(z - x)\|},$$

which gives the result. \square

APPENDIX C. SECOND-ORDER DIFFERENTIATION OF ENTROPIC POTENTIALS

This section is dedicated to the proof of Proposition 4.1, that states that the series of spherical harmonics of \mathbf{u}_ε belongs to ℓ_1 .

C.1. Euclidean second-order derivatives. Note that one can find in [24] expressions for first-order and second-order derivatives of the cost c . The next proposition gives second-order partial derivatives of the potential \mathbf{u}_ε .

Proposition C.1. *The potential \mathbf{u}_ε is twice-differentiable everywhere, and*

$$\frac{\partial^2 \mathbf{u}_\varepsilon}{\partial x_i \partial x_j}(x) = \int \tilde{c}_{ij}(x, z) \exp\left(\frac{\mathbf{u}_\varepsilon(x) - c(x, z) + \mathbf{u}_\varepsilon^{c, \varepsilon}(z)}{\varepsilon}\right) d\nu(z) + \frac{\partial_{x_i} \mathbf{u}_\varepsilon(x) \partial_{x_j} \mathbf{u}_\varepsilon(x)}{\varepsilon},$$

where

$$\tilde{c}_{ij}(x, z) = \frac{\partial^2 c(x, z)}{\partial x_i \partial x_j} - \frac{\partial_{x_i} c(x, z) \partial_{x_j} c(x, z)}{\varepsilon}.$$

Besides, the same holds for $\mathbf{u}_\varepsilon^{c, \varepsilon}$ and

$$\frac{\partial^2 \mathbf{u}_\varepsilon^{c, \varepsilon}}{\partial z_i \partial z_j}(z) = \int \tilde{c}_{ij}(z, x) \exp\left(\frac{\mathbf{u}_\varepsilon(x) - c(x, z) + \mathbf{u}_\varepsilon^{c, \varepsilon}(z)}{\varepsilon}\right) d\nu(z) + \frac{\partial_{z_i} \mathbf{u}_\varepsilon^{c, \varepsilon}(z) \partial_{z_j} \mathbf{u}_\varepsilon^{c, \varepsilon}(z)}{\varepsilon}.$$

Proof. The same calculus can be found in [28][Lemma 3], up to the fact that one can recognize partial derivatives of \mathbf{u}_ε , that is (B.2), in the result, at the very end of our proof. First of all, g_ε is bounded by using [64][Lemma 2.1] and the compactness of \mathbb{S}^2 . Thus, one can differentiate in (B.2) under the integral sign, and

$$(C.1) \quad \frac{\partial^2 \mathbf{u}_\varepsilon}{\partial x_i \partial x_j}(x) = \int \partial_{x_j} z_i g_\varepsilon(x, z) d\nu(z).$$

In view of using classical rules of differentiation, note that $z_i g_\varepsilon(x, z) = (\partial_{x_i} c(x, z)) G(x, z)$, for

$$G(x, z) = \exp\left(\frac{\mathbf{u}_\varepsilon(x) - c(x, z) + \mathbf{u}_\varepsilon^{c, \varepsilon}(z)}{\varepsilon}\right).$$

Besides,

$$\partial_{x_j} G(x, z) = \frac{1}{\varepsilon} G(x, z) \partial_{x_j} (\mathbf{u}_\varepsilon(x) - c(x, z)).$$

As a byproduct,

$$(C.2) \quad \begin{aligned} \partial_{x_j} z_i g_\varepsilon(x, z) &= \frac{\partial^2 c(x, z)}{\partial x_i \partial x_j} G(x, z) + \partial_{x_i} c(x, z) \frac{1}{\varepsilon} G(x, z) \left(\partial_{x_j} \mathbf{u}_\varepsilon(x) - \partial_{x_j} c(x, z) \right), \\ (C.3) \quad &= G(x, z) \left(\frac{\partial^2 c(x, z)}{\partial x_i \partial x_j} + \partial_{x_i} c(x, z) \frac{\partial_{x_j} \mathbf{u}_\varepsilon(x) - \partial_{x_j} c(x, z)}{\varepsilon} \right). \end{aligned}$$

Plugging (C.3) in (C.1) and using that $z_i g_\varepsilon(x, z) = (\partial_{x_i} c(x, z)) G(x, z)$ when rearranging,

$$\begin{aligned} \frac{\partial^2 \mathbf{u}_\varepsilon}{\partial x_i \partial x_j}(x) &= \int G(x, z) \left(\frac{\partial^2 c(x, z)}{\partial x_i \partial x_j} - \frac{\partial_{x_i} c(x, z) \partial_{x_j} c(x, z)}{\varepsilon} \right) + \frac{\partial_{x_j} \mathbf{u}_\varepsilon(x)}{\varepsilon} z_i g_\varepsilon(x, z) d\nu(z), \\ &= \int G(x, z) \left(\frac{\partial^2 c(x, z)}{\partial x_i \partial x_j} - \frac{\partial_{x_i} c(x, z) \partial_{x_j} c(x, z)}{\varepsilon} \right) d\nu(z) + \frac{1}{\varepsilon} \partial_{x_i} \mathbf{u}_\varepsilon(x) \partial_{x_j} \mathbf{u}_\varepsilon(x). \end{aligned}$$

where we also used the explicit derivatives of \mathbf{u}_ε from (B.2). The Hessian of $\mathbf{u}_\varepsilon^{c,\varepsilon}$ follows by symmetry. \square

C.2. Proof of Proposition 4.1. From Proposition C.1, \mathbf{u}_ε is twice-differentiable everywhere, that gives us the continuity of \mathbf{Q}_ε , and of $\partial_{x_i}\mathbf{u}_\varepsilon$. In the expression of the second-order partial derivatives given in (C.1), the term $\frac{1}{\varepsilon}\partial_{x_i}\mathbf{u}_\varepsilon(x)\partial_{x_j}\mathbf{u}_\varepsilon(x)$ is thus continuous. The remaining term takes the form of a parameter-dependant integral, whose integrand is continuous and bounded. Thus, the result follows by a direct application of the theorem for continuity under the integral sign, and by using the property that a sequence of spherical harmonics belongs to ℓ_1 for functions that are twice continuously differentiable, see [43][Theorem 2].

REFERENCES

- [1] C. AGOSTINELLI AND M. ROMANAZZI, *Nonparametric analysis of directional data based on data depth*, Environmental and ecological statistics, 20 (2013), pp. 253–270.
- [2] J. AMEIJERAS-ALONSO AND R. M. CRUJEIRAS, *Directional statistics for wildfires*, in Applied directional statistics, Chapman and Hall/CRC, 2018, pp. 203–226.
- [3] V. BARNETT, *The ordering of multivariate data*, Journal of the Royal Statistical Society: Series A (General), 139 (1976), pp. 318–344.
- [4] J. BEIRLANT, S. BUITENDAG, E. DEL BARRIO, M. HALLIN, AND F. KAMPER, *Center-outward quantiles and the measurement of multivariate risk*, Insurance: Mathematics and Economics, 95 (2020), pp. 79–100.
- [5] B. BERCU AND J. BIGOT, *Asymptotic distribution and convergence rates of stochastic algorithms for entropic optimal transportation between probability measures*, The Annals of Statistics, 49 (2021), pp. 968 – 987.
- [6] B. BERCU, J. BIGOT, AND G. THURIN, *Stochastic optimal transport in banach spaces for regularized estimation of multivariate quantiles*, SIAM Journal on Mathematics of Data Science, 7 (2025), pp. 1664–1689.
- [7] E. BERNTON, P. GHOSAL, AND M. NUTZ, *Entropic optimal transport : Geometry and large deviations*, Duke Mathematical Journal, 171 (2022), pp. 3363–3400.
- [8] F. BIGL, G. FRAUX, N. J. BROWNING, AND M. CERIOTTI, *Fast evaluation of spherical harmonics with sphericart*, The Journal of Chemical Physics, 159 (2023).
- [9] G. CARLIER, V. CHERNOZHUKOV, G. DE BIE, AND A. GALICHON, *Vector quantile regression and optimal transport, from theory to numerics*, Empirical Economics, 62 (2022), pp. 35–62.
- [10] P. CHAUDHURI, *On a geometric notion of quantiles for multivariate data*, Journal of the American statistical association, 91 (1996), pp. 862–872.
- [11] V. CHERNOZHUKOV, A. GALICHON, M. HALLIN, AND M. HENRY, *Monge–Kantorovich depth, quantiles, ranks and signs*, The Annals of Statistics, 45 (2017), pp. 223 – 256.
- [12] G. S. CHIRIKJIAN AND A. B. KYATKIN, *Engineering applications of noncommutative harmonic analysis: with emphasis on rotation and motion groups*, CRC press, 2000.
- [13] S. COHEN, B. AMOS, AND Y. LIPMAN, *Riemannian convex potential maps*, in International Conference on Machine Learning, PMLR, 2021, pp. 2028–2038.
- [14] D. CORDERO-ERAUSQUIN, R. J. MCCANN, AND M. SCHMUCKENSCHLÄGER, *A riemannian interpolation inequality à la borell, brascamp and lieb*, Inventiones mathematicae, 146 (2001), pp. 219–257.
- [15] M. CUTURI, *Sinkhorn distances: Lightspeed computation of optimal transport*, Advances in Neural Information Processing Systems, 26 (2013).

- [16] M. CUTURI, M. KLEIN, AND P. ABLIN, *Monge, Bregman and occam: Interpretable optimal transport in high-dimensions with feature-sparse maps*, vol. 202 of Proceedings of Machine Learning Research, 2023, pp. 6671–6682.
- [17] M. CUTURI AND G. PEYRÉ, *Computational optimal transport*, Foundations and Trends® in Machine Learning, 11 (2019), pp. 355–607.
- [18] E. DEL BARRIO, A. GONZÁLEZ SANZ, AND M. HALLIN, *Nonparametric multiple-output center-outward quantile regression*, Journal of the American Statistical Association, (2024), pp. 1–43.
- [19] P. DELANOE AND G. LOEPER, *Gradient estimates for potentials of invertible gradient-mappings on the sphere*, Calculus of Variations and Partial Differential Equations, 26 (2006), pp. 297–311.
- [20] H. DEMNI, A. MESSAOUD, AND G. C. PORZIO, *The cosine depth distribution classifier for directional data*, Applications in Statistical Computing: From Music Data Analysis to Industrial Quality Improvement, (2019), pp. 49–60.
- [21] H. DEMNI AND G. C. PORZIO, *Directional dd-classifiers under non-rotational symmetry*, in 2021 IEEE International Conference on Multisensor Fusion and Integration for Intelligent Systems (MFI), 2021, pp. 1–6.
- [22] J.-L. DORTET-BERNADET AND N. WICKER, *Model-based clustering on the unit sphere with an illustration using gene expression profiles*, Biostatistics, 9 (2008), pp. 66–80.
- [23] Y. FAN, M. HENRY, B. PASS, AND J. A. RIVERO, *Lorenz map, inequality ordering and curves based on multidimensional rearrangements*. arXiv, 2022.
- [24] O. FERREIRA, A. IUSEM, AND S. NÉMETH, *Concepts and techniques of optimization on the sphere*, Top, 22 (2014), pp. 1148–1170.
- [25] J. FEYDY, T. SÉJOURNÉ, F.-X. VIALARD, S.-I. AMARI, A. TROUVÉ, AND G. PEYRÉ, *Interpolating between optimal transport and mmd using sinkhorn divergences*, in The 22nd International Conference on Artificial Intelligence and Statistics, PMLR, 2019, pp. 2681–2690.
- [26] M. FRUNGILLO, *Discrete approximation of optimal transport on compact spaces*, arXiv preprint arXiv:2401.14538, (2024).
- [27] E. GARCÍA-PORTUGUÉS, D. PAINDAVEINE, AND T. VERDEBOUT, *On optimal tests for rotational symmetry against new classes of hyperspherical distributions*, Journal of the American Statistical Association, 115 (2020), pp. 1873–1887.
- [28] A. GENEVAY, *Entropy-regularized Optimal Transport for Machine Learning*, PhD thesis, Université Paris sciences et lettres, 2019.
- [29] A. GENEVAY, M. CUTURI, G. PEYRÉ, AND F. BACH, *Stochastic Optimization for Large-scale Optimal Transport*, Advances in neural information processing systems, 29 (2016).
- [30] P. GHOSAL AND B. SEN, *Multivariate ranks and quantiles using optimal transport: Consistency, rates, and nonparametric testing*, The Annals of Statistics, 50 (2022), pp. 1012–1037.
- [31] A. K. GHOSH AND P. CHAUDHURI, *On maximum depth and related classifiers*, Scandinavian Journal of Statistics, 32 (2005), pp. 327–350.
- [32] Z. GOLDFELD, K. KATO, G. RIOUX, AND R. SADHU, *Limit theorems for entropic optimal transport maps and sinkhorn divergence*, Electronic Journal of Statistics, 18 (2024), pp. 980–1041.
- [33] M. HALLIN, *From mahalanobis to bregman via monge and kantorovich: Towards a “general generalized distance”*, Sankhya B, 80 (2018), pp. 135–146.
- [34] M. HALLIN, *Measure Transportation and Statistical Decision Theory*, Annual Review of Statistics and Its Application, 9 (2022), pp. 401–424.
- [35] M. HALLIN, E. DEL BARRIO, J. CUESTA-ALBERTOS, AND C. MATRÁN, *Distribution and quantile functions, ranks and signs in dimension d: A measure transportation approach*, The Annals of Statistics, 49 (2021), pp. 1139 – 1165.

- [36] M. HALLIN AND H. LIU, *Quantiles and quantile regression on riemannian manifolds: a measure-transportation-based approach*, arXiv preprint arXiv:2410.15711, (2024).
- [37] M. HALLIN, H. LIU, AND T. VERDEBOUT, *Nonparametric measure-transportation-based methods for directional data*, Journal of the Royal Statistical Society Series B: Statistical Methodology, (2024).
- [38] M. HALLIN AND G. MORDANT, *Center-outward multiple-output lorenz curves and gini indices a measure transportation approach*, working papers ecares, ULB – Universite Libre de Bruxelles, 2022.
- [39] M. HALLIN, D. VECCHIA, AND H. LIU, *Rank-based testing for semiparametric var models: A measure transportation approach*, Bernoulli, 29 (2023).
- [40] B. F. HAMFELDT AND A. G. TURNQUIST, *A convergence framework for optimal transport on the sphere*, Numerische Mathematik, 151 (2022), pp. 627–657.
- [41] K. HAUCH AND C. REDENBACH, *Quantiles and depth for directional data from elliptically symmetric distributions*, arXiv preprint arXiv:2210.06098, (2022).
- [42] S. HUNDRIESER, M. KLATT, AND A. MUNK, *The Statistics of Circular Optimal Transport*, Springer Nature Singapore, Singapore, 2022, pp. 57–82.
- [43] H. KALF, *On the expansion of a function in terms of spherical harmonics in arbitrary dimensions*, Bulletin of the Belgian Mathematical Society-Simon Stevin, 2 (1995), pp. 361–380.
- [44] O. D. KELLOGG, *Foundations of potential theory*, vol. 31, Springer Science & Business Media, 2012.
- [45] D. KONEN AND D. PAINDAVEINE, *Spatial quantiles on the hypersphere*, The Annals of Statistics, 51 (2023), pp. 2221–2245.
- [46] S. KUNIS AND D. POTTS, *Fast spherical fourier algorithms*, Journal of Computational and Applied Mathematics, 161 (2003), pp. 75–98.
- [47] C. LEY, C. SABBABH, AND T. VERDEBOUT, *A new concept of quantiles for directional data and the angular mahalanobis depth*, Electronic Journal of Statistics [electronic only], 8 (2014).
- [48] C. LEY AND T. VERDEBOUT, *Modern directional statistics*, CRC Press, 2017.
- [49] ———, *Applied directional statistics: modern methods and case studies*, CRC Press, 2018.
- [50] R. Y. LIU, *On a notion of data depth based on random simplices*, The Annals of Statistics, (1990), pp. 405–414.
- [51] R. Y. LIU, J. M. PARELIUS, AND K. SINGH, *Multivariate analysis by data depth: descriptive statistics, graphics and inference, (with discussion and a rejoinder by liu and singh)*, The annals of statistics, 27 (1999), pp. 783–858.
- [52] R. Y. LIU AND K. SINGH, *Ordering directional data: concepts of data depth on circles and spheres*, The Annals of Statistics, 20 (1992), pp. 1468–1484.
- [53] G. LOEPER, *Regularity of optimal maps on the sphere: The quadratic cost and the reflector antenna*, Archive for rational mechanics and analysis, 199 (2011), pp. 269–289.
- [54] G. LOEPER AND C. VILLANI, *Regularity of optimal transport in curved geometry: The nonfocal case*, Duke Mathematical Journal, 151 (2010), pp. 431 – 485.
- [55] K. V. MARDIA AND P. E. JUPP, *Directional statistics*, vol. 2, Wiley Online Library, 2000.
- [56] D. MARINUCCI, D. PIETROBON, A. BALBI, P. BALDI, P. CABELLA, G. KERKYACHARIAN, P. NATOLI, D. PICARD, AND N. VITTORIO, *Spherical needlets for cosmic microwave background data analysis*, Monthly Notices of the Royal Astronomical Society, 383 (2008), pp. 539–545.
- [57] S. B. MASUD, M. WERENSKI, J. M. MURPHY, AND S. AERON, *Multivariate soft rank via entropic optimal transport: sample efficiency and generative modeling*, Journal of Machine Learning Research, 24 (2023), pp. 1–65.
- [58] R. J. MCCANN, *Polar factorization of maps on riemannian manifolds*, Geometric & Functional Analysis GAFA, 11 (2001), pp. 589–608.

- [59] N. MIOLANE, N. GUIGUI, A. L. BRIGANT, J. MATHE, B. HOU, Y. THANWERDAS, S. HEYDER, O. PELTRE, N. KOEP, H. ZAATITI, H. HAJRI, Y. CABANES, T. GERALD, P. CHAUCHAT, C. SHEWMAKE, D. BROOKS, B. KAINZ, C. DONNAT, S. HOLMES, AND X. PENNEC, *Geomstats: A python package for riemannian geometry in machine learning*, Journal of Machine Learning Research, 21 (2020), pp. 1–9.
- [60] K. MOSLER, *Depth statistics*, Robustness and complex data structures: Festschrift in Honour of Ursula Gather, (2013), pp. 17–34.
- [61] S. NAGY, H. DEMNI, D. BUTTARAZZI, AND G. C. PORZIO, *Theory of angular depth for classification of directional data*, Advances in Data Analysis and Classification, (2023).
- [62] S. NAGY AND P. LAKETA, *Theoretical properties of angular halfspace depth*, arXiv preprint arXiv:2402.08285, (2024).
- [63] Z. NIU AND B. B. BHATTACHARYA, *Distribution-free joint independence testing and robust independent component analysis using optimal transport*. arXiv, 2022.
- [64] M. NUTZ AND J. WIESEL, *Entropic optimal transport: convergence of potentials*, Probability Theory and Related Fields, 184 (2022), pp. 401–424.
- [65] G. PANDOLFO AND A. D’AMBROSIO, *Clustering directional data through depth functions*, Computational Statistics, 38 (2023), pp. 1487–1506.
- [66] G. PANDOLFO, D. PAINDAVEINE, AND G. C. PORZIO, *Distance-based depths for directional data*, Canadian Journal of Statistics, 46 (2018), pp. 593–609.
- [67] M. PEGORARO, S. VEDULA, A. A. ROSENBERG, I. TALLINI, E. RODOLÀ, AND A. BRONSTEIN, *Vector quantile regression on manifolds*, in ICML Workshop on New Frontiers in Learning, Control, and Dynamical Systems, 2023.
- [68] A. PEWSEY AND E. GARCÍA-PORTUGUÉS, *Recent advances in directional statistics*, Test, 30 (2021), pp. 1–58.
- [69] A.-A. POOLADIAN AND J. NILES-WEED, *Entropic estimation of optimal transport maps*, 2021.
- [70] P. J. ROUSSEEUW AND A. STRUYF, *Characterizing angular symmetry and regression symmetry*, Journal of Statistical Planning and Inference, 122 (2004), pp. 161–173.
- [71] P. SAAVEDRA-NIEVES AND R. M. CRUJEIRAS, *Nonparametric estimation of directional highest density regions*, Advances in Data Analysis and Classification, 16 (2022), pp. 761–796.
- [72] V. SEGUY, B. B. DAMODARAN, R. FLAMARY, N. COURTY, A. ROLET, AND M. BLONDEL, *Large-Scale Optimal Transport and Mapping Estimation*, in ICLR 2018 - International Conference on Learning Representations, 2018, pp. 1–15.
- [73] R. SERFLING, *Depth functions in nonparametric multivariate inference*, DIMACS Series in Discrete Mathematics and Theoretical Computer Science, 72 (2006), p. 1.
- [74] H. SHI, M. DRTON, M. HALLIN, AND F. HAN, *Center-outward sign- and rank-based quadrant, spearman, and kendall tests for multivariate independence.*, working papers ecares, ULB – Université Libre de Bruxelles, 2021.
- [75] H. SHI, M. DRTON, AND F. HAN, *Distribution-free consistent independence tests via center-outward ranks and signs*, Journal of the American Statistical Association, 117 (2022), pp. 395–410.
- [76] C. G. SMALL, *Measures of centrality for multivariate and directional distributions*, Canadian Journal of Statistics, 15 (1987), pp. 31–39.
- [77] A. STROMME, *Sampling from a schrödinger bridge*, in International Conference on Artificial Intelligence and Statistics, PMLR, 2023, pp. 4058–4067.
- [78] J. W. TUKEY, *Mathematics and the picturing of data*, Proceedings of the International Congress of Mathematicians (Vancouver, B. C., 1974), 2 (1975), pp. 523–531.
- [79] A. VACHER AND F.-X. VIALARD, *Convex transport potential selection with semi-dual criterion*, in Advances in Neural Information Processing Systems, 2022.

- [80] C. VILLANI, *Topics in optimal transportation*, vol. 58 of Graduate Studies in Mathematics, American Mathematical Society, 2003.
- [81] M. VOLKER, *Lectures on constructive approximation: Fourier, spline, and wavelet methods on the real line, the sphere, and the ball*, Springer Science & Business Media, 2012.
- [82] G. T. VON NESSI, *On the regularity of optimal transportation potentials on round spheres*, *Acta applicandae mathematicae*, 123 (2013), pp. 239–259.
- [83] H. WELLER, P. BROWNE, C. BUDD, AND M. CULLEN, *Mesh adaptation on the sphere using optimal transport and the numerical solution of a monge–ampère type equation*, *Journal of Computational Physics*, 308 (2016), pp. 102–123.
- [84] M. A. WIECZOREK AND M. MESCHÉDE, *Shtools: Tools for working with spherical harmonics*, *Geochemistry, Geophysics, Geosystems*, 19 (2018), pp. 2574–2592.
- [85] Y. ZUO AND R. SERFLING, *General notions of statistical depth function*, *The Annals of Statistics*, (2000), pp. 461–482.